Thermoprotection by a cell membrane-localized metacaspase in a green alga

Yong Zou[1#*], Igor Sabljić[1#], Natalia Horbach[2#], Adrian N. Dauphinee[1#], Anna Åsman[1], Lucia Sancho Temino[1], Marcin Drag[2], Simon Stael[1], Marcin Poreba[2], Jerry Ståhlberg[1] and Peter V. Bozhkov[1*]

[1]Department of Molecular Sciences, Uppsala BioCenter, Swedish University of Agricultural Sciences and Linnean Center for Plant Biology, Uppsala, Sweden

[2]Department of Chemical Biology and Bioimaging, Wroclaw University of Science and Technology, Wroclaw, Poland

[#] These authors contributed equally to this work

[*]Authors for correspondence: Yong.Zou@slu.se and Peter.Bozhkov@slu.se

The authors responsible for distribution of materials integral to the findings presented in this article in accordance with the policy described in the Instructions for Authors (https://academic.oup.com/plcell/pages/General-Instructions) are: Yong Zhou (Yong.Zou@slu.se) and Peter V. Bozhkov (Peter.Bozhkov@slu.se)

Short title: Thermoprotection by a metacaspase

Abstract

Caspases are restricted to animals, while other organisms, including plants possess metacaspases (MCAs), a more ancient and broader class of structurally-related yet biochemically distinct proteases. Our current understanding of plant MCAs is derived from studies in streptophytes, and mostly in Arabidopsis expressing nine MCAs with partly redundant activities. In contrast to streptophytes, most chlorophytes contain only one or two hitherto uncharacterized MCAs, providing an excellent platform for MCA research. Here we investigate CrMCA-II, a single type II MCA from a model chlorophyte *Chlamydomonas reinhardtii*. Surprisingly, unlike other studied MCAs and similar to caspases, CrMCA-II dimerizes both *in vitro* and *in vivo*. Furthermore, activation of CrMCA-II *in vivo* correlates with the dimerization. Most of CrMCA-II in the cell is present as a zymogen attached to the plasma membrane (PM). Deletion of *CrMCA-II* by CRISPR/Cas9 compromises thermotolerance leading to increased cell death under heat stress. Adding back either wild-type or catalytically dead CrMCA-II restores thermoprotection, suggesting that its proteolytic activity is dispensable for this effect. Finally, we link the non-proteolytic role of CrMCA-II in thermotolerance to the ability to modulate PM fluidity. Our study reveals an ancient, MCA-dependent thermotolerance mechanism retained by Chlamydomonas and probably lost during the evolution of multicellularity.

42 **Introduction**

43 In 1992 the first caspase was discovered, interleukin-1β-converting enzyme (ICE), better
44 known as caspase-1 (Cerretti et al., 1992; Thornberry et al., 1992), and shortly thereafter, the
45 *Caenorhabditis elegans* cell death gene *ced-3* (Yuan et al., 1993) was identified, heralding a
46 flurry of research on caspases that continues to this day (Julien and Wells, 2017; Van
47 Opdenbosch and Lamkanfi, 2019; Kesavardhana et al., 2020; Ross et al., 2022). However,
48 caspases are a relatively small and mostly animal-specific part of a large superfamily of
49 cysteine proteases (C14 within the CD clan), all sharing a caspase-like structural fold and
50 found throughout all kingdoms of life (Uren et al., 2000; Minina et al., 2020). Among them,
51 eukaryotic metacaspases (MCAs) and prokaryotic MCA-like proteases form the
52 phylogenetically broadest group, with members found in all living organisms except animals
53 (Tsiatsiani et al., 2011; McLuskey and Mottram, 2015; Minina et al., 2017; Klemenčič and
54 Funk, 2019). Despite structural similarity between MCAs and caspases, the two groups of
55 proteases fundamentally differ in their substrate specificity, with MCAs, unlike Asp-specific
56 caspases, cleaving exclusively after positively charged (Arg or Lys) residues (Vercammen et
57 al., 2004; Sundström et al., 2009; Minina et al., 2020).
58
59 Whereas all known eukaryotic MCAs contain both p20- (catalytic) and p10-like conserved
60 regions, they are classified into three major types based on the presence of additional protein
61 modules and the relative position of the p20 and p10 regions (Minina et al., 2020). Thus, the
62 distinguishing feature of type I MCAs is the N-terminal pro-domain. Type II MCAs are
63 distinguished by the presence of a long linker separating p20 and p10 regions, whereas type
64 III MCAs are defined by swapping of the two regions, so that the p10 is located N-terminally
65 to the catalytic p20 region. Notably, there is a significant variation in the amino acid
66 sequence, length of distinct protein regions and occurrence of additional motifs among MCAs
67 of the same type, in particular for type I that is presumably responsible for the differences in
68 their biochemical properties and physiological functions (Klemenčič and Funk, 2019).
69 However, further structure-function categorization of the members within each MCA type is
70 not possible today due to a limited success in structural analysis of these enzymes, with only
71 three type I (*Trypanosoma brucei* TbMCA-Ib/MCA2, *Saccharomyces cerevisiae* ScMCA-
72 I/MCA1/YCA1 and *Candida glabrata* CgMCA-I) and two type II (*Arabidopsis thaliana*
73 AtMCA-IIa/MC4 and AtMCA-IIf/MC9) MCA crystal structures available (McLuskey et al.,
74 2012; Wong et al., 2012; Zhu et al., 2020; Conchou et al., 2022; Stael et al., 2023).
75

76 Among the three types of MCAs, type I is found in all non-animal organisms, while type II is
77 specific for Chloroplastida (originally named Viridiplantae, Latin for "green plants") and type
78 III for Heterokontophyta (phytoplanktonic protists; (Choi and Berges, 2013; Minina et al.,
79 2017; Klemenčič and Funk, 2019). Thus, the vast majority of annotated green plant genomes
80 encode both type I and type II MCAs. Green plants form a monophyletic taxon comprising
81 both land plants and green algae re-distributed into two evolutionary lineages, the
82 Chlorophyta (chlorophytes) and Streptophyta (streptophytes), that diverged over a billion
83 years ago (Bemer, 1985; Morris et al., 2018). While the chlorophytes comprise only green
84 algae, the streptophytes include both land plants and the remaining green algae (called
85 "streptophyte algae"; Becker and Marin, 2009).
86
87 Research on plant MCAs has so far almost exclusively concerned streptophytes and was
88 dominated by the use of Arabidopsis, due to its advantages of being a genetically tractable
89 model system and having a relatively well-understood biology. The Arabidopsis MCA family
90 consists of nine genes, three of type I (AtMC1-AtMC3 or AtMCA-Ia - AtMCA-Ic, according
91 to original or updated nomenclature, respectively) and six of type II (AtMC4 - AtMC9 or
92 AtMCA-IIa - AtMCA-IIf), the latter including four tandem duplicated genes (AtMC4 -
93 AtMC7 or AtMCA-IIa - AtMCA-IId; (Vercammen et al., 2004; Minina et al., 2020).
94 Arabidopsis MCAs are involved in the regulation of immune and stress responses, aging and
95 programmed cell death (Coll et al., 2010; Watanabe and Lam, 2011; Bollhöner et al., 2013;
96 Coll et al., 2014; Hander et al., 2019; Shen et al., 2019; Wang et al., 2021; Li et al., 2022). For
97 recent reviews on Arabidopsis MCAs see Minina et al., (2017), Salguero-Linares and Coll
98 (2019) and Huh (2022). The absence of strong developmental or fitness phenotypes of single
99 *MCA* gene knockouts in Arabidopsis points to some degree of redundancy among different
100 MCAs (Tsiatsiani et al., 2011; Huh, 2022). Furthermore, while some of the MCA-dependent
101 proteolytic functions might be isoform-specific, it is not easy to prove that experimentally.
102 Indeed, MCAs have rather loose substrate cleavage specificity for residues in P2, P3, and P4
103 positions (Vercammen et al., 2006; Sundström et al., 2009; Tsiatsiani et al., 2013). This
104 complicates ascribing a given physiological response or developmental event to the
105 proteolytic cleavage of a target protein substrate by a particular MCA, since there is a mixture
106 of MCAs with similar substrate specificity in a cell (or cell lysate).
107
108 With these arguments in mind, we turned our attention to the chlorophyte lineage of green
109 plants whose sequenced genomes reveal mostly one or two *MCA* genes (*vs* several in

110 streptophytes; Tsiatsiani et al., 2011), providing a powerful paradigm for plant MCA research.
111 Despite this obvious advantage, there is to date no genetic evidence for the involvement of
112 MCAs in chlorophyte biology, thus precluding evolutionary insight into the MCA-dependent
113 functions in green plants.
114
115 We set out to establish chemical and genetic toolboxes for exploring MCAs in a chlorophyte,
116 *Chlamydomonas reinhardtii* (hereafter Chlamydomonas). Chlamydomonas is a unicellular
117 green alga used as a model organism by virtue of having a greatly reduced number of cell
118 types and simplified cell-to-cell communications, as compared to e.g. Arabidopsis (Gutman
119 and Niyogi, 2004), and combining key animal (e.g. cell motility) and plant (e.g.
120 photosynthesis) characteristics (Merchant et al., 2007). The genome of Chlamydomonas
121 encodes one type I and one type II MCA named according to the current nomenclature
122 (Minina et al., 2020), CrMCA-I and CrMCA-II, respectively. Such genetic simplicity renders
123 Chlamydomonas a favourable model for uncovering primordial roles of the two types of
124 MCAs. Here we report biochemical and functional studies of CrMCA-II. Unlike other MCAs,
125 CrMCA-II can oligomerize both *in vitro* and *in vivo*. It is predominantly present as a
126 zymogen, associated with plasma membrane (PM), but translocates to the cytoplasm upon
127 heat stress (HS). Genetic experiments combined with live-cell imaging revealed that CrMCA-
128 II plays a protease-independent cytoprotective role under HS, presumably related to its ability
129 to module PM fluidity.
130

131 **Results**

132 **Phylogenetic analysis places two Chlamydomonas MCAs at the base of the evolutionary**
133 **tree**

134 BLAST search revealed that species in the order Chlamydomonadales, including
135 Chlamydomonas, *Volvox carteri* and *Gonium pectorale*, contain one type I and one type II
136 MCA. Some green algae, e.g. *Raphidocelis subcapitata* and *Auxenochlorella protothecoides*,
137 are completely devoid of type II and contain only type I MCAs. To gain insight into the
138 evolutionary position of Chlamydomonas MCAs, we performed a phylogenetic analysis of
139 MCA sequences from green plants with well-annotated genomes. The analysis demonstrated
140 that both Chlamydomonas MCAs, CrMCA-I and CrMCA-II, as well as other chlorophyte
141 MCAs are situated at the bases of evolutionary clusters comprising type I and type II MCAs
142 from green plants (Supplemental Figure S1).
143

144 **CrMCA-II is a Ca^{2+}- and redox-dependent arginine-specific protease**

145 We purified bacterially expressed recombinant His-tagged CrMCA-II (rCrMCA-II) using a
146 HisTrap column followed by size exclusion chromatography (SEC). For reasons discussed
147 later, the optimal buffer used for CrMCA-II proteolytic activity measurements and as a basis
148 for further studies was 50 mM Tris pH 7.5, 25 mM NaCl, 20 mM $CaCl_2$, 0.1% CHAPS and
149 7.5 mM DTT. Similar to all hitherto studied MCAs, rCrMCA-II was unable to cleave after
150 Asp (Figure 1A). However, unlike other MCAs, rCrMCA-II displayed a strict preference for
151 Arg over Lys at the P1 position in the tetrapeptide substrates, with only trace hydrolytic
152 activity against Lys-containing substrates (Figure 1A).
153

154 As with the majority of MCAs, rCrMCA-II required millimolar concentrations of Ca^{2+} for
155 activation (Supplemental Figure S2A). An inhibitory effect of zinc on CrMCA-II
156 (Supplemental Figure S2B) was not as strong as that for the spruce mcII-Pa (Bozhkov et al.,
157 2005), but similar to human caspase 8 (Stennicke and Salvesan, 1997). rCrMCA-II was active
158 at neutral pH, with an optimum at pH 7.5 (Supplemental Figure S2C), and as expected, was
159 highly sensitive to arginal protease inhibitors (Supplemental Figure S2D).
160

161 Noteworthy, rCrMCA-II critically required reducing agents for activation (Supplemental
162 Figure S2E), exhibiting dose-dependent activity with increasing concentration of DTT up to
163 20 mM (Figure 1B). The predicted structure of the CrMCA-II catalytic center revealed
164 Cys329 in the vicinity of catalytic Cys141 (5.4 Å, Supplemental Figure S3), at a distance even

closer than the distance between the catalytic dyad of Cys141 and His87 (6.5 Å), pointing to a possibility of a Cys-Cys bridge formation that could inhibit catalytic activity. However, the rCrMCA-II^{C329A} mutant was significantly less proteolytically active than the WT enzyme and still required reducing conditions for the activity (Supplemental Figure S2F). In agreement with the results obtained for rCrMCA-II, addition of DTT to Chlamydomonas cell lysates prepared from the control (UVM4) strain increased Arg-specific proteolytic activity and hydrogen peroxide had an opposing effect (Supplemental Figure S4). Collectively, these results demonstrate that CrMCA-II is a Ca^{2+}- and redox-dependent arginine-specific protease.

CrMCA-II oligomerizes *in vitro* and *in vivo*

Interestingly, SEC profile of rCrMCA-II in the buffer without DTT and Ca^{2+} displayed two peaks, corresponding to the monomeric (43.5 kDa) and dimeric (87 kDa) forms (Figure 1C). When subjected to SDS-PAGE, both monomer- and dimer-containing SEC fractions displayed full-length protein and autocleavage fragments of a similar molecular mass (Figure 1D). The dimerization was confirmed by Yeast Two-Hybrid (Y2H) assay (Figure 1E). Caspases dimerize through the sixth β-sheet located in the p10 region (MacKenzie and Clark, 2012). We attempted to identify the interaction region of CrMCA-II, but neither p20 nor p10 or linker regions could interact with the full-length CrMCA-II in the Y2H assay (Supplemental Figure S5), indicating that either the corresponding protein fragments are misfolded or the presence of two or even all three regions is required for the dimerization.

The SEC fractions containing either monomeric or dimeric forms of rCrMCA-II were proteolytically active in the buffer supplemented with DTT and Ca^{2+} (Figure 1C, insert). As DTT may prevent protein-protein interaction by disrupting intermolecular disulfide bonds, the activity of the dimer-containing fraction may in fact be caused by monomers forming upon addition of DTT. Indeed, we observed a decreased dimer-to-monomer ratio when 1mM DTT was added to the SEC buffer, confirming that DTT induces dimer-to-monomer transition (Figure 1C). This was further confirmed using native gel electrophoresis (Figure 1F). To unequivocally determine which of the two forms of rCrCMA-II represent catalytically active protease, we performed an in-gel activity assay wherein monomeric and dimeric forms of rCrMCA-II were subjected to native electrophoresis followed by the addition of Ac-VRPR-AMC. Both monomers and dimers were able to cleave the fluorescent substrate (Figure 1G), demonstrating that dimerization is dispensable for rCrMCA-II activation *in vitro*.

199 To investigate whether CrMCA-II dimerizes *in vivo*, we performed SEC of total protein
200 extract from a knockout Chlamydomonas strain complemented with HA-tagged WT CrMCA-
201 II (CrMCA-II-3×HA; generation of transgenic strains is discussed later), followed by SDS-
202 PAGE and immunoblot analysis of the SEC fractions with anti-HA (Figure 1H). The analysis
203 identified three major forms of CrMCA-II-3×HA co-existing in the cell extract: monomer
204 (peak fraction 81), dimer (peak fraction 73) and a megadalton-scale complex (peak fraction
205 43; Figure 1H). While CrMCA-II-3×HA in the SEC fractions containing monomer and
206 megadalton complex was present mainly as a zymogen (i.e. full-length protein), the dimer-
207 containing fractions were represented by the autoprocessed, mature protease, generating a
208 p10-fragment under denatured conditions that is recognized by α-HA (Figure 1H). This
209 fragment results from the autocleavage at a conserved site (after Arg190 in case of CrMCA-II
210 and based on sequence alignment with known cleavage sites from Arabidopsis type II MCAs)
211 within the linker region of type II MCAs (Zhu et al., 2020; Supplemental Figure S6. Besides
212 three major forms of CrMCA-II-3×HA, the SEC analysis of the total protein extract has also
213 revealed an abundance of a C-terminal fragment smaller than the p10-fragment present in a
214 free, unbound form (peak fraction 87; Figure 1H) and apparently representing a product of
215 self-degradation (Watanabe and Lam, 2011).
216
217 Since endogenous CrMCA-II exists as monomeric, dimeric and large (megadalton-scale)
218 species, we asked whether these species are proteolytically active in the substrate cleavage
219 assay, at two contrasting levels of Ca^{2+}, but otherwise maintaining optimal buffer conditions:
220 (i) without adding any exogenous Ca^{2+}, and (ii) with addition of 20 mM $CaCl_2$. While the first
221 conditions approximate the chemical environment *in situ*, with only a basal level of cell-
222 derived Ca^{2+} present in the assay, the second conditions provide optimal level of Ca^{2+} for
223 detecting full activity of a proteolytically competent CrMCA-II. Ca^{2+} supplementation
224 strongly enhanced VRPRase activity of the SEC fractions with monomeric and megadalton
225 CrMCA-II species, largely represented by zymogen, but inhibited activity of dimer-containing
226 fractions represented by the autoprocessed mature enzyme (Figure 1I). As expected, the SEC
227 fractions containing a C-terminal fragment of CrMCA-II smaller than p10 displayed only
228 trace activity, independently of the Ca^{2+} level (Figure 1I).
229
230 Results of SEC, immunoblotting and proteolytic activity assays together have two important
231 implications. First, the pattern of the CrMCA-II protein in SDS-PAGE can be used as a proxy
232 to its proteolytic competence. Second, it is highly likely that it is a dimer representing a

233 proteolytically active form of CrMCA-II *in vivo*, whereas monomeric and megadalton
234 CrMCA-II species are present as catalytically competent but inactive zymogen molecules.
235
236 **Development of CrMCA-II specific chemical probes**
237 To determine substrate specificity of CrMCA-II beyond P1 position and to develop optimal
238 substrates, hybrid combinatorial substrate library (HyCoSuL) screening combining both
239 natural and unnatural amino acids, was employed (Poreba et al., 2017). Using the library with
240 fixed Arg at the P1 position, the enzyme preferences at the P2, P3 and P4 positions were
241 screened (Supplemental Figure S7). A broad substrate specificity was found for rCrMCA-II
242 from P4 to P2 positions. Nevertheless, to get a better insight into enzyme preferences, a set of
243 individual tetrapeptide substrates bearing a 7-Amino-4-carbamoylmethylcoumarin (ACC)
244 fluorophore reporter were synthesized and subjected to rCrMCA-II hydrolysis (Figure 2A-C;
245 Supplemental Figure S8; Supplemental Table S1). This screening enabled to identify two
246 substrates, one composed of natural amino acids, Ac-His-Arg-Thr-Arg-ACC (Ac-HRTR-
247 ACC), and one with unnatural amino acids, Ac-His(Bzl)-hSer(Bzl)-Thr-Arg-ACC (Ac-
248 H(Bzl)-hS(Bzl)-TR-ACC), both of which show a high cleavage rate by rCrMCA-II. The
249 catalytic activity of rCrMCA-II on these substrates was significantly higher than that on the
250 commercially available and commonly used MCA and paracaspase substrate Ac-VRPR-ACC
251 (Table 1, Figure 2B, C), which was designed from the optimal substrate preference of
252 Arabidopsis AtMCA-IIf/MC9 (Vercammen et al., 2006), making them efficient probes for
253 measuring CrMCA-II activity.
254
255 **Table 1** The catalytic activity of rCrMCA-II against three selected substrates

Substrate	**K_M, μM**	**k_{cat}, s^{-1}**	**k_{cat}/K_M, $M^{-1}s^{-1}$**
Ac-Val-Arg-Pro-Arg-ACC	56.5	10.3	1.82×10^5
Ac-His-Arg-Thr-Arg-ACC	48.1	15.9	3.31×10^5
Ac-His(Bzl)-hSer(Bzl)-Thr-Arg-ACC	31.0	13.0	4.20×10^5

256
257 A considerable benefit of analyzing protease substrate preferences using HyCoSuL
258 technology is the development of a peptide that perfectly fits to the active site of the
259 investigated enzymes. Therefore, the rCrMCA-II preferred peptidic substrates were further
260 used to design fluorescently labeled activity-based probes (ABPs), *viz.* covalent inhibitors that
261 bind to the enzyme active site in an irreversible manner. To do this, we labeled HRTR and
262 H(Bzl)-hS(Bzl)-TR peptides with a cyanine 5 (Cy5) tag through an 6-aminohexanoic acid

263 (Ahx) linker to separate the fluorophore and peptide. We selected the acyloxymethyl ketone
264 group (AOMK) to use as the warhead (Figure 2D), as this electrophile is known to covalently
265 react with the catalytic Cys residue of Cys proteases (Kato et al., 2005). In such a manner, we
266 developed two CrMCA-II ABPs, Cy5-ahx-HRTR-AOMK and Cy5-ahx-H(Bzl)-hS(Bzl)-TR-
267 AOMK (Figure 2D and Supplemental Figure S9.
268
269 To determine whether the ABPs can differentiate between WT and catalytically dead mutant
270 of CrMCA-II, as well as between mature WT CrMCA-II and its zymogen, we incubated
271 purified rCrMCA-II or rCrMCA-II^{C141A} with Cy5-ahx-HRTR-AOMK under optimal buffer
272 conditions in the presence or absence of Ca^{2+} followed by SDS-PAGE. As shown in Figure
273 2E, no labelling was observed for rCrMCA-II^{C141A} with or without Ca^{2+}, whereas the ABP
274 labelled only the autoprocessed, mature form of rCrMCA-II generated in the presence of Ca^{2+}
275 in a dose dependent manner. This indicates that the ABP can distinguish between active
276 rCrMCA-II and zymogen. The fragment of mature rCrMCA-II covalently bound by the Cy5
277 probe is expected to include the p20 region as well as a part of the linker to Arg190, migrating
278 as a band of ~ 25 kDa (Figure 2E). These results demonstrate that our Cy5-labeled ABPs are
279 useful tools for detecting mature CrMCA-II enzyme.
280
281 **Generation of *CrMCA-II* knockout (KO) mutants and complementation strains**
282 To study physiological roles of CrMCA-II, we generated *crmca-ii* mutant strains using the
283 recently established targeted insertional mutagenesis method based on the CRISPR/Cas9
284 system (Picariello et al., 2020). We obtained three strains (*ii-4*, *ii-9* and *ii-23*) lacking
285 *CrMCA-II* expression. PCR amplification of genomic DNA from strains *ii-9* and *ii-23* with a
286 pair of primers flanking the insertion site furnished a product of around 3.5 kbp (*vs.* 1.8 kbp in
287 the control strain, Figure 3A, B). Sequencing confirmed the insertion of AphVIII cassette
288 conferring paromomycin resistance in the genomic DNA (Supplemental Figure S10). A third
289 mutant, *ii-4* showed no product after colony PCR (Figure 3B), indicating a larger insertion.
290
291 Quantitative PCR (qPCR) has been adapted for estimating gene copy number in a genome, as
292 an alternative to a more time-consuming Southern blot (Hoebeeck et al., 2007). Accordingly,
293 we used this method for assessing insertion events during genome editing. While *ii-9* and *ii-*
294 *23* strains contained a single *AphVIII* gene copy, confirming single insertion events, *ii-4*
295 presumably had two *AphVIII* gene copies inserted into the genome (Figure 3C, D).

296 Furthermore, qPCR analysis confirmed that none of the three *crmca-ii* mutant strains
297 contained an intact *CrMCA-II* gene (Figure 3C).
298
299 To verify a lack of the CrMCA-II protein in the generated mutants, we used an antibody
300 raised against a 16 amino acid-long peptide from the p10 region of CrMCA-II (Supplemental
301 Figure S11A). The antibody recognized both the zymogen (~ 42.4 kDa) and a fragment
302 composed of p10 and a part of the linker region generated *via* autocleavage (migrated as ~ 25
303 kDa but estimated to be 22 kDa) on immunoblots of total protein extracts isolated from the
304 control strain (UVM4; Figure 3E and Supplemental Figure S11B). In contrast, none of the
305 three *crmca-ii* strains revealed the presence of CrMCA-II protein (Figure 3E and
306 Supplemental Figure S11B), indicating that all three strains were KO mutants. We also
307 analyzed cell lysates isolated from the control strain and KO mutants for proteolytic activity
308 of CrMCA-II using the optimized substrate Ac-HRTR-ACC. To minimize risk that cleavage
309 of this substrate by other Chlamydomonas proteases could mask the effect of CrMCA-II
310 deficiency, we blocked activity of aspartate, cysteine and serine proteases, except for arginal
311 proteases, using a combination of aprotinin, pepstatin A, PMSF and Pefabloc SC. While
312 HRTRase activity was readily detected in the lysates from UVM4 strain, it was nearly absent
313 in the lysates from the *crmca-ii* strains (Figure 3F and Supplemental Figure S11C), making
314 them a robust tool for functional studies.
315
316 To further expand our toolbox, we cloned the native *CrMCA-II* promoter and genomic DNA
317 of *CrMCA-II* into MoClo system (Crozet et al., 2018), and obtained mutant strains
318 complemented with HA-tagged WT CrMCA-II or catalytically dead CrMCA-II^{C141A} (Figure
319 3D). While complementation with WT enzyme furnished mature, catalytically active
320 protease, complementation with autoprocessing-deficient CrMCA-II^{C141A} could not restore
321 HRTRase activity in cell lysates (Figure 3E, F).
322
323 **CrMCA-II plays cytoprotective role under heat stress (HS) independent of its protease**
324 **activity**
325 We took advantage of the generated probes and algal strains to explore the role of CrMCA-II
326 *in vivo*. To begin, we compared cell growth of UVM4 and mutant strains under normal
327 conditions (TAP medium, pH 7.0, 23°C) and different types of abiotic stress, including salt
328 stress, nitrogen, phosphorous or acetate starvation, high (pH 8.4) or low (pH 6.0) pH stress,
329 and HS (42°C). We only observed a significant difference in the growth rate under HS, with

330 *crmca-ii* strains exhibiting suppressed growth as compared to UVM4 (data not shown). We
331 then compared the frequency of cell death in UVM4, *crmca-ii* and complemented strains after
332 60-min HS at 42°C using fluorescein diacetate (FDA) staining. We found that the mutant
333 strains had a higher frequency of cell death than the UVM4 strain (Figure 4A). Consistently,
334 complementation with WT CrMCA-II restored cell viability. Surprisingly, two independent
335 strains complemented with CrMCA-II^{C141A} did so too (Figure 4A), demonstrating that the
336 cytoprotective effect of CrMCA-II under HS conditions is independent of its protease activity.
337
338 Next, we wondered what happened to CrMCA-II during 42°C HS at the transcriptional and
339 protein levels. We found that while HS led to a steady decrease of the *CrMCA-II* transcript
340 level in the UVM4 strain (Figure 4B), it promoted zymogen accumulation without
341 significantly altering the abundance of the mature form of the enzyme, detected through the
342 formation of p10 fragment recognized by α-CrMCA-II (Figure 4C; Supplemental Figure
343 S11B). In agreement, HRTRase activity of cell lysates remained constant over the 60-min
344 duration of HS treatment (Figure 4D). These data indicated that HS triggered a *trans*-acting
345 mechanism and/or conformational changes suppressing CrMCA-II activation and leads to
346 zymogen accumulation. To clarify this further, we measured HRTRase activity of purified
347 rCrMCA-II pretreated for 5 min in Ca^{2+}- and DTT-free buffer (non-permissive conditions) at
348 various temperatures ranging from 24°C to 42°C and observed a decrease in the activity with
349 increased pre-treatment temperature following addition of Ca^{2+} and DTT (Figure 4E). We
350 thus assumed that heat-induced suppression of CrMCA-II activation could be due to
351 conformational changes of the zymogen.
352
353 **CrMCA-II is associated with the plasma membrane (PM) but translocates to the**
354 **cytoplasm during HS**
355 Given the thermoprotective role of CrMCA-II, we wondered where it was located in a
356 Chlamydomonas cell before and after onset of HS. For studying subcellular localization of
357 CrMCA-II, we assembled an expression vector with a constitutive P_{PSAD} promoter, gDNA of
358 *CrMCA-II*, mVenus tag and T_{PSAD} terminator. After transformation into UVM4 cells (Neupert
359 et al., 2009), we obtained a strain overexpressing CrMCA-II with a C-terminal mVenus tag,
360 that we named CrMCA-II-overexpressor 14-3 (OE14-3). Confocal microscopy analysis of
361 unstressed OE14-3 showed a strong mVenus signal co-localized with FM4-64-stained plasma
362 membrane (PM, Figure 5A). PM localization of CrMCA-II-mVenus was confirmed using
363 strain CC-4533, distinguished from UVM4 by the presence of both an intact cell wall and

364 flagella (Supplemental Figure S12), suggesting that this localization is a strain-independent
365 characteristic of Chlamydomonas.
366
367 To provide independent biochemical evidence for the PM localization of CrMCA-II, proteins
368 from several fractions including cytosolic, low-density membrane [LDM, including PM and
369 endomembranes (EM)], and separated PM and EM (Supplemental Figure S13) were
370 immunoblotted with antibodies against CrMCA-II and H^+ ATPase, a marker for PM (Norling
371 et al., 1996). As expected, H^+ ATPase was enriched in the PM fraction, which also displayed
372 a strong accumulation of CrMCA-II, in agreement with the microscopy data (Figure 5B, left
373 blot). Although confocal microscopy failed to detect cytoplasmic CrMCA-II-mVenus signal
374 in unstressed cells (Figure 5A), the concentrated soluble protein fraction (precipitated and
375 dissolved in the same volume as LDM fraction) exhibited a similar level of CrMCA-II as
376 LDM fraction (Figure 5B, right). Interestingly, CrMCA-II in the PM fraction was present only
377 as a zymogen, in contrast to the cytosolic and EM fractions containing both zymogen and
378 mature enzyme (represented by p10 fragment; Figure 5B). Taken together, these results
379 confirm PM localization of CrMCA-II in unstressed cells, but also point to the existence of
380 the cytoplasmic pool of the protein. In addition, the data suggest that while the PM pool of
381 CrMCA-II is represented exclusively by zymogen, the cytoplasmic pool is partitioned
382 between zymogen and mature protease.
383
384 The localization of CrMCA-II under HS was studied using a strain overexpressing mCherry
385 fused to simian virus 40 nuclear localization signal (SV40), in the OE14-3 background. We
386 observed that when mid-log grown cells were exposed to HS at 42°C for 60 min, a strong
387 mVenus signal appeared in the perinuclear cytoplasm (Figure 5C). Thus, the ratio of PM to
388 cytoplasmic fluorescent signals of CrMCA-II was decreased by more than two times in the
389 heat-treated compared to unstressed cells (Figure 5D, E). Importantly, proteolytic activity of
390 CrMCA-II was not required for its PM-to-cytoplasm re-distribution, as revealed by the
391 microscopy analysis of a strain expressing mVenus tagged CrMCA-II^{C141A} (Supplemental
392 Figure S14A-C).
393
394 Next, to determine whether the HS-induced accumulation of the cytoplasmic CrMCA-II is a
395 consequence of its translocation from the PM or *de novo* protein synthesis, the cells were
396 treated with cycloheximide (CHX), an inhibitor of translation (Schneider-Poetsch et al.,
397 2010), prior to HS. Since CHX could not prevent or alleviate perinuclear signal

398 (Supplemental Figure S14D, E), we conclude that enhanced cytoplasmic accumulation of
399 CrMCA-II during HS is a result of PM-to-cytoplasm translocation rather than *de novo* protein
400 synthesis.
401
402 HS is known to induce the influx of Ca^{2+} through PM (Saidi et al., 2009). MCAs generally
403 contain two Ca^{2+} binding sites, one with high affinity and unknown function and another with
404 low affinity and involved in catalytic activation (Klemenčič and Funk, 2019). During HS,
405 Ca^{2+} influx results in an increase of intracellular Ca^{2+} concentration to a micromolar level
406 (summarized in Schroda et al., 2015), i.e. to the range where MCAs bind Ca^{2+} with high
407 affinity. To test whether the influx of Ca^{2+} through PM is involved in the PM-to-cytoplasm
408 translocation of CrMCA-II, log-phase OE14-3 cells were pre-treated with Ca^{2+} chelators 0.75
409 mM EGTA or 1,2-bis(o-aminophenoxy) ethane-N,N,N,N′-tetraacetic acid (BAPTA) prior to
410 HS. Calcium chelation led to a moderate but statistically significant suppression of the
411 CrMCA-II translocation, whereas addition of excess Ca^{2+} to the EGTA-treated cells fully
412 reverted that effect (Figure 5E), suggesting that Ca^{2+} influx during HS does play a role in the
413 PM-to-cytoplasm translocation of CrMCA-II.
414
415 **CrMCA-II modulates PM fluidity**
416 We hypothesized that the molecular mechanism underlying the cytoprotective effect of
417 CrMCA-II under HS might be related to its potential role in modulating PM fluidity, a
418 dynamic property of PM critically involved in HS signaling (Saidi et al., 2009; Niu and
419 Xiang, 2018) and activation of cell death (Tekpli et al., 2013). To address this hypothesis, we
420 stained the algal strains with DiOC6(3), a lipophilic green fluorescent dye with a high affinity
421 to Chlamydomonas PM (Long et al., 2016), followed by a fluorescence recovery after photo-
422 bleaching (FRAP) assay. An attempt of running the assay at 42°C failed due to
423 hypersensitivity of the heat-treated cells to the PM photobleaching that resulted in cell
424 collapse, so we reduced the HS temperature to 39°C.
425
426 We did not observe any significant differences in the proportion of the initial signal recovery
427 of DiOC6(3) on the PM between different strains and regardless of the temperature (data not
428 shown). However, CrMCA-II deficiency led to a strong decrease of signal recovery rate (*viz.*
429 $T_{1/2}$ increase) of DiOC6(3) in unstressed cells, as compared to UVM4 and both WT and
430 CrMCA-II^{C141A} complementation strains (Figure 5F). While UVM4 and complementation
431 strains generally responded to HS by a mild increase in the PM fluidity, this increase was

432 significantly augmented in the CrMCA-II deficient mutant (Figure 5F, Supplemental Figure
433 S15). These results indicate that CrMCA-II controls PM fluidity by preventing PM
434 rigidization in unstressed conditions, which also enables to avoid the hyperfluidization in
435 response to HS. Similar to cytoprotection and PM localization, this function of CrMCA-II
436 occurs independently of its protease activity.
437

438 **Discussion**

439

440 **Oligomerization of CrMCA-II**

441 The absence of oligomerization-dependent activation of MCAs has been proposed as a
442 generic feature distinguishing them from caspases and paracaspases (McLuskey and Mottram,
443 2015; Minina et al., 2020). Our observations with Chlamydomonas CrMCA-II are not fully
444 consistent with this notion. Firstly, bacterially expressed CrMCA-II can form monomers and
445 dimers, which are both catalytically active (Figure 1C, D, G). While dimerization in this case
446 may be due to a high concentration of the recombinant protein, the results of Y2H assay do
447 not support this assumption (Figure 1E). Secondly, Chlamydomonas protein extracts contain
448 monomeric, dimeric and megadalton-size CrMCA-II species, of which only dimers seem to
449 be fully active (Figure 1H, I).

450

451 Our observation that dimerization of endogenous CrMCA-II correlates with the autocleavage
452 yielding the p10 fragment (Figure 1H) is in agreement with a hypothetical model for type II
453 MCA maturation, which postulated that autocleaved MCA molecules could form a
454 catalytically active homodimer (Lam and Zhang, 2012). One cannot completely rule out a
455 possibility that protein species from Chlamydomonas cell extracts with a molecular mass
456 corresponding to CrMCA-II dimer and recognized by specific antibody are in fact
457 heterodimers composed of CrMCA-II and not an unknown protein of a similar molecular
458 mass, although the likelihood of such scenario is low.

459

460 The structural details of CrMCA-II dimerization remain unknown. While type II MCAs have
461 a similar β-strand arrangement with caspases, the L2 loop is embedded in the potential
462 dimerization interface, making it impossible for the dimerization to occur in the same way as
463 in caspases (Zhu et al., 2020). However, unlike caspases, type II MCAs have a long,
464 intrinsically disordered linker between the p20 and p10 regions (Supplemental Figure S3),
465 providing an alternative interface for dimerization. Although we failed to detect interaction
466 between the individually expressed linker and the full-length CrMCA-II in the Y2H assay
467 (Supplemental Figure S5), this could be due to large conformational changes of the disordered
468 linker in yeast. Structural data for catalytically mature CrMCA-II are required to
469 unambiguously determine which structural elements serve as the dimerization interface, as
470 well as molecular topology of the dimer. Likewise, structure-function understanding of the

471 megadalton-scale, CrMCA-II zymogen-containing complex identified in Chlamydomonas
472 extracts awaits further studies.
473
474 **CrMCA-II is a redox-dependent protease**
475 Reducing conditions are crucial for CrMCA-II activation both *in vitro* (Supplemental Figure
476 S2E) and in cell lysates (Supplemental Figure S4), and at the same time stimulate dimer-to-
477 monomer transition of rCrMCA-II (Figure 1E), suggesting that Cys-Cys disulfide bond(s)
478 might contribute to the CrMCA-II dimerization. The redox-regulated activity of a type III
479 MCA from the marine diatom *Phaeodactylum tricornutum* was previously found to correlate
480 with the formation of a disulfide bond between Cys202 and Cys259 (Graff van Creveld et al.,
481 2021). While these Cys residues are not conserved in CrMCA-II (not shown), we reasoned
482 that the formation of a disulfide bond between catalytic Cys141 and the closely situated
483 Cys329 would explain strict requirement of reducing conditions for the protease activity of
484 CrMCA-II (Supplemental Figure S3). However, Cys329Ala mutation did not render protease
485 activity independent of the reducing agent (Supplemental Figure S2F), calling for further
486 research to uncover an underlying mechanism and its physiological implications *in vivo*.
487
488 Noteworthy, strong redox dependence of CrMCA-II proteolytic activity revealed in our study
489 is consistent with the appearance of CrMCA-II in the published redox thiol proteome datasets
490 of Chlamydomonas (Pérez-Pérez et al., 2017; McConnell et al., 2018). Furthermore, redox
491 dependence might be an important regulatory mechanism related to CrMCA-II location on the
492 PM; a major site for ROS production, perception and signal transduction in a cell (Nordzieke
493 and Medraño-Fernandez, 2018), and responsible for thermotolerance and other physiological
494 functions of this MCA yet to be identified.
495
496 **Substrate specificity of CrMCA-II**
497 Without regard to the non-proteolytic role in thermotolerance, mature CrMCA-II exhibits a
498 multifold higher preference for Arg than for Lys at the P1 position in tetrapeptide substrates
499 (Figure 1A), implying that the S1 binding pocket of CrMCA-II has a higher affinity for Arg
500 than for Lys (Stael et al., 2023). Whether or not this holds true *in vivo* is unknown and
501 necessitates information about cleavage sites in the native targets. In fact, strong preference
502 for Arg over Lys in peptidic substrates is a common feature of MCAs (Minina et al., 2017),
503 which however, is not obvious when analyzing cleavage sites of the target proteins

504 (Sundström et al., 2009; Tsiatsiani et al., 2013). This suggests that the residues at P1' to P4'
505 of the substrates may also affect the binding and activity of MCAs during cleavage.
506
507 As for a specificity beyond P1, CrMCA-II displayed a clear preference for a basic amino acid
508 at P3 site (Supplemental Figure S7), similar to Arabidopsis AtMCA-IIf/MC9 (Vercammen et
509 al., 2006). Accordingly, substitution of Arg for Asp at P3 of the commercially available
510 VRPR-based substrate greatly diminished proteolytic activity of CrMCA-II (Figure 2B).
511 However, unlike AtMCA-IIf, which prefers Pro, Tyr or Phe at P2 and branched chain Ile or
512 Val at P4 site (Vercammen et al., 2006), CrMCA-II instead favours substrates with Ala, Thr
513 or Ser at P2 and His or Ser at P4 (Supplemental Figure S7). This comparison implies that
514 while MCAs have rather loose P2-P4 substrate specificity, it differs among different class
515 members.
516
517 The ABPs designed from the substrate specificity screening are useful tools for detecting
518 catalytically active proteoforms of the recombinantly produced CrMCA-II (Figure 2D, E).
519 Theoretically, these ABPs could also be used to detect active CrMCA-II *in vivo*. However, we
520 were thus far unable to find suitable conditions for microscopy to differentiate the Cy5 signal
521 between UVM4 and *crmca-ii* mutant, presumably due to low abundance of the mature
522 protease in the cells. An alternative explanation is poor permeability of the Cy5 probe to the
523 pool(s) of active CrMCA-II. Therefore, further optimization of the chemical structure of these
524 ABPs to improve permeability, as well as screening for physiologically relevant conditions
525 facilitating CrMCA-II activation are both required for live imaging of CrMCA-II activity in a
526 cell.
527
528 **PM localization and the thermoprotective role of CrMCA-II**
529 MCAs feature diverse subcellular localization patterns, but most are nucleocytoplasmic and
530 can be found in both soluble (cytosolic) and insoluble (protein aggregates and endoplasmic
531 reticulum) protein fractions (Huh, 2022). Localization of CrMCA-II on PM is thus uncommon
532 and therefore intriguing. The only other known MCA with similar localization validated
533 experimentally is a *Trypanosoma brucei* TbMCA-Id/MCA4 of type I — a pseudopeptidase
534 lacking catalytic Cys (Proto et al., 2011). Both CrMCA-II and TbMCA-Id/MCA4 are devoid
535 of transmembrane domain(s), pointing to their strong affinity to lipids and/or other
536 membranal proteins. Accordingly, TbMCA-Id/MCA4 has been shown to undergo *N*-
537 myristoylation and palmitoylation *in vivo* to become associated with the internal surface of

538 flagellar membrane (Proto et al., 2011). Being devoid of a *N*-myristoylation motif, the Cr-
539 MCA-II sequence yet contains a number of predicted palmitoylation motifs (Ning et al., 2020;
540 data not shown), which might contribute to the PM localization of the protein.
541
542 Interestingly, the presence of transmembrane domains is a widespread feature among
543 orthocaspases and type I MCAs in prokaryotes (Klemenčič and Funk, 2018; La et al., 2022).
544 Furthermore, transmembrane domains are predicted to occur (DeepTMHMM, Hallgren et al.,
545 2022), albeit with much lower frequency, in type I MCAs from unicellular green algae,
546 including *Auxenochlorella protothecoides* 0710 and *Picochlorum sp*. It thus seems likely that
547 direct association with the PM is an ancient feature of C14 proteases, which was preserved by
548 prokaryotes and some single celled eukaryotes but lost during the evolution of
549 multicellularity. The latter assumption, however, is not completely true, since animal caspase-
550 8 was shown to dimerize and become activated upon assembly of death inducing signaling
551 complex (DISC) at the PM during initiation of the extrinsic pathway of apoptosis (Feig et al.,
552 2007). Apart from the proteolytic role in apoptosis, caspase-8 promotes adhesion and Erk
553 signaling in neuroblastoma cells *via* recruiting PM-associated Src tyrosine kinase (Finlay and
554 Vuori, 2007). Notably, this function of caspase-8 is independent of its catalytic activity,
555 resembling the non-catalytic role of CrMCA-II revealed in the current study. Nonetheless, in
556 contrast to CrMCA-II, both procaspase-8 (zymogen) and mature caspase-8 enzyme are
557 present only in the cytosolic S-100 fraction and are absent in the light and heavy membrane
558 fractions (Breckenridge et al., 2002; Figure 5B).
559
560 As only the full-length zymogen but not processed CrMCA-II is present at the PM, while the
561 cytosol and the endomembranes contain both types of proteoforms (Figure 5B), there must be
562 a tight spatial control over protease activity of CrMCA-II in a cell. Thus, PM could serve as a
563 compartment sequestering zymogen, whereas CrMCA-II protease maturation and substrate
564 cleavage might take place in the cytoplasm. Given the critical requirement of Ca^{2+} for
565 CrMCA-II activation and that the endoplasmic reticulum (ER) is a Ca^{2+} storage seat with a
566 high concentration (Stael et al., 2011), it is reasonable to assume that the proteolytic function
567 of CrMCA-II (if any) is fulfilled in or around the ER when Ca^{2+} is released. However, testing
568 a panel of knockout and complementation strains under varied environmental settings failed
569 to identify conditions wherein Chlamydomonas growth was dependent on the protease
570 activity of CrMCA-II.
571

572 The PM plays a fundamental role in intra- and intercellular communication and in response to
573 adverse environmental conditions, serving also as a crucial component of cell repair
574 machinery (Horn and Jaiswal, 2019; Jaillais and Ott, 2019). The non-proteolytic role of the
575 PM-localized CrMCA-II zymogen in HS could be related to its ability to modulate PM
576 fluidity, alleviating hypofluidity under normal conditions and, correspondingly, preventing a
577 large-amplitude hyperfluidity response to high temperatures (see model in Figure 6). Indeed,
578 changes in PM fluidity have been shown to play a causative role in or correlate with various
579 types of cell death in animals (summarized in Tekpli et al., 2013). In Chlamydomonas,
580 treatment with membrane rigidifier DMSO decreases cell viability (Haire et al., 2018).
581 Accordingly, the hypofluid PM in *crmca-ii* strains may fail to support transient lipid mobility
582 after heat injury, undermining cell repair and leading to increased cell death (Horn and
583 Jaiswal, 2019).
584
585 In contrast to animals (Shuba, 2021), heat response in plants remains poorly characterized. It
586 is postulated that both streptophytes and chlorophytes sense heat *via* an increase in PM
587 fluidity causing activation of the cyclic nucleotide-gated ion channels and controlled entry of
588 extracellular Ca^{2+} to the cytosol, which further leads to the heat shock factor (HSF)-mediated
589 transcriptional response and biosynthesis of necessary proteins, such as heat shock proteins
590 (HSPs) (Mittler et al., 2012; Cano-Ramirez et al., 2021; Guihur et al., 2022). We initially
591 thought that the compromised thermotolerance of *crmca-ii* strains was associated with
592 aberrant HS sensing at the level of HSF and HSP production, but did not observe any
593 differences in the transcript levels of HSFs and major HSPs known to execute HS response in
594 Chlamydomonas (Zhang et al., 2022) between UVM4 and *crmca-ii* (data not shown). We
595 therefore conclude that the mechanism of CrMCA-II-dependent thermoprotection is restricted
596 to the regulation of physico-chemical properties of the PM *per se* affecting its fluidity, bilayer
597 stability and hence functionality upon temperature shift (Horváth et al., 2008).
598
599 There are multiple factors underlying changes in PM fluidity, such as the alterations in the
600 conformation of integral membrane proteins, density and size of lipid rafts, and saturation
601 level of phospholipids (Desai and Miller, 2018; Pozza et al., 2022). Which of these factors are
602 controlled or mediated by CrMCA-II will be addressed in our future work that will include
603 characterization of CrMCA-II interactome and, specifically, zymogen-containing megadalton-
604 scale complex (Figure 1G), as well as lipidomics analysis of the *crmca-ii* strains. Intriguingly,
605 CrMCA-II is predicted to harbour several intrinsically disordered segments, spanning the non-

606 catalytic regions of the protein (data not shown). Moreover, CrMCA-II has been recently
607 identified as a part of a heat-resistant intrinsically disordered proteome of Chlamydomonas
608 (Zhang et al., 2018). This observation together with our findings that the heat treatment
609 stabilizes the zymogen and inhibits proteolytic activity of rCrMCA-II (Figure 4C-E) reinforce
610 genetic evidence for a non-proteolytic role of rCrMCA-II in thermotolerance.
611
612 Interestingly, HS induces PM-to-cytoplasm translocation of CrMCA-II, in a Ca^{2+} influx-
613 dependent manner (Figures 5C-E and 6). According to recent structural data obtained for
614 Arabidopsis AtMCA-IIa/MC4 (Zhu et al., 2020), Ca^{2+} could bind to the high affinity-binding
615 pocket of CrMCA-II (Asp95, Asp97, Glu98, and Asp100; Supplemental Figure S3), and
616 impose structural changes causing its detachment from the PM. Whether PM-to-cytoplasm
617 translocation of CrMCA-II has any functional role in HS response remains an open question.
618
619 In conclusion, CrMCA-II, - a single type II MCA of Chlamydomonas, - confers
620 thermotolerance *via* a mechanism governing PM fluidity, which is completely independent of
621 its protease activity. In this respect, the non-catalytic mode of CrMCA-II action is reminiscent
622 of that of ScMCA-I/MCA1/YCA1, a single MCA encoded by *Saccharomyces cerevisiae*
623 genome, in suppressing protein aggregate formation (also under HS) and replicative aging,
624 albeit catalytic Cys276 mutant of the yeast MCA1 could only partially rescue *mca1* deletion
625 phenotypes (Lee et al., 2010; Hill et al., 2014). Taken together, the findings in budding yeast
626 and Chlamydomonas suggest an evolutionary scenario wherein the ancient primordial role of
627 the MCAs was to carry out quality control both in the cytoplasm (e.g., to counteract protein
628 aggregation) and at the cell surface (e.g., to maintain membrane fluidity) for fitness and
629 survival of unicellular organisms in fluctuating environments. Complete or partial
630 independence of intricately-regulated proteolytic activity could provide additional robustness
631 to the proposed role of MCAs.
632

633 **Methods**

634

635 **Strains and culture conditions**

636 Unless stated otherwise, UV mutagenesis strain 4 (UVM4), with high efficiency to
637 overexpress foreign genes (Neupert et al., 2009), was used as a control strain. The
638 Chlamydomonas cells were grown in tris-acetate-phosphate (TAP) medium at 23°C and a
639 light-dark cycle (LD16:8). The cells were harvested at a density of $1\text{-}2\times10^{7}$ cells mL^{-1}.

640

641 **Phylogenetic analysis**

642 The MCA sequences of green algae and higher plants were obtained from Phytozome 13
643 (https://phytozome.jgi.doe.gov/pz/portal.html). The MEGA X (Kumar et al., 2018) was used
644 to perform alignment with embedded Muscle program and phylogenetic analysis with default
645 setting for neighbour-joining method.

646

647 **rCrMCA-II expression and purification**

648 rCrMCA-II was expressed using a codon-optimized construct in *E. coli* and then purified
649 through affinity chromatography and size exclusion chromatography (SEC) as described
650 (Sabljić et al., 2022).

651

652 **Protease activity assay of rCrMCA-II**

653 The proteolytic activity of 5 ng purified rCrMCA-II was measured in the reaction buffer (*viz.*
654 optimal buffer conditions: 50 mM Tris pH 7.5, 25 mM NaCl, 20 mM $CaCl_2$, 0.1% CHAPS,
655 and 7.5 mM DTT), with 50 µM VRPR-AMC as a substrate, unless stated otherwise.
656 Fluorescence intensity was measured every minute using BMG Labtech POLARstar Omega
657 Microplate Readers at excitation/emission 360–380 nm/440–460 nm. The activity was
658 determined based on the slope of at least 10 recordings.

659

660 **rCrMCA-II protease activity assay in native electrophoresis**

661 To perform native electrophoresis, a 4-20% gradient stain-free gel was loaded with protein
662 aliquots that had been incubated with 7.5 mM DTT for 15 min at 4°C. Controls were treated
663 the same way, but without DTT. The gel was then run at 150 V, for 45 min in Tris/Glycine
664 buffer. After gel running, 3 mL of the DTT-free reaction buffer was added on top of the gel
665 and fluorescence was detected using a BioRad Gel Doc EZ Imager programmed for ethidium
666 bromide.

667

668 **SEC of Chlamydomonas total protein extract**

669 Cells were harvested in the late log phase from 100 mL TAP medium and suspended in 1mL
670 extraction buffer (50 mM Tris pH 7.5, 25-100 mM NaCl, 1 mM EDTA, 1% glycerol, 1 µM
671 Aprotinin, 10 µM Pepstatin A, 1 mM PMSF and 2 mM Pefabloc SC). The cell mixture was
672 sonicated for 3 min by 10-sec pulses, with 5-sec intervals and the cell debris was pelleted at
673 17,000 *g* for 20 min. The resulting crude cell extract was filtered through a 0.45-µm filter
674 before loading onto a HiLoad 16/60 Superdex 200 pg column (GE Healthcare) at 4°C. A
675 buffer containing 50 mM Tris (pH 7.5) and 25 mM NaCl was used for equilibration and
676 elution, and elution profiles were recorded at 280 nm. Fractions of 750 µL were collected,
677 precipitated with 90% methanol (Bychkov et al., 2011), and dissolved in 40 µL 1 × SDS
678 sample buffer. Immunoblots were performed after separating 10 µL of each fraction by SDS-
679 PAGE in a 4-20% gel. A set of protein standards was used as a reference for calibration and
680 determination of the molecular mass of CrMCA-II protein species in the samples.

681

682 **Chemical reagents**

683 All chemicals used for the synthesis of substrates and activity-based probes (ABPs) were
684 purchased from commercial suppliers and used without purification unless otherwise noted.
685 The Rink amide RA resin (loading 0.48 mmol g^{-1}) was used for the synthesis of ACC-labeled
686 substrates, and the 2-chlorotrityl chloride resin (1.59 mmol g^{-1}, 100-200 mesh) was used for
687 the synthesis of peptides that were further converted into ABPs (both resins were from Iris
688 Biotech GmbH, Germany). Fmoc-protected amino acids (all > 98% pure) were purchased
689 from various suppliers: Iris Biotech GmbH, Creosalus, P3 BioSystems, QM Bio, Bachem.
690 N,N-diisopropylethylamine (DIPEA, peptide grade), diisopropylcarbodiimide (DICI, peptide
691 grade), piperidine (PIP, peptide grade), and trifluoroacetic acid (TFA, purity 99%) were all
692 from Iris Biotech, GmbH. 2,4,6-trimethylpyridine (2,4,6-collidine, peptide grade),
693 triisopropylsilane (TIPS, purity 99%), 2,2,2-trifluoroethanol (TFE), anhydrous
694 tetrahydrofuran (THF), hydrogen bromide (30% wt. in AcOH), 4-methylmorpholine (NMM),
695 isobutylchloroformate (IBCF), and 2,6-dimethylbenzoic acid (2,6-DMBA) were all purchased
696 from Sigma Aldrich. N-hydroxybenzotriazole (HOBt, monohydrate) was from Creosalus.
697 HATU and HBTU (both peptide grade) were from ChemPep Inc.. N,N`-dimethylformamide
698 (DMF, peptide grade) and acetonitrile (ACN, HPLC pure) were from WITKO Sp. z o.o.,
699 Poland. Methanol (MeOH, pure for analysis), dichloromethane (DCM, pure for analysis),
700 diethyl ether (Et_2O, pure for analysis), acetic acid (AcOH, 98% pure) and phosphorus

701 pentoxide (P_2O_5, 98% pure) were from POCh, Poland. Cyanine-5 NHS was purchased from
702 Lumiprobe. Diazomethane was generated according to the Aldrich Technical Bulletin (AL-
703 180) protocol.
704
705 **Characterization of rCrMCA-II P4-P2 substrate specificity using HyCoSuL**
706 To determine the CrMCA-II specificity in the P4-P2 positions, we used the P1-Arg HyCoSuL
707 library (Poreba et al., 2017). P4, P3, and P2 sub-libraries were each screened at 100 µM final
708 concentration in 100 µL final volume with rCrMCA-II. The active enzyme was in the 2-10
709 nM range, depending on the sub-library used. The screening time was 30 min, but for each
710 substrate cleavage only the linear portion of the progression curve (10-15 min) was used for
711 the analysis (RFU sec^{-1} calculation) to avoid problems of substrate consumption. Screening of
712 each library was performed at least in triplicate, and the average value was used to create the
713 rCrMCA-II specificity matrix (S.D. for each substrate was below 15%). The hydrolysis rate
714 for the best recognized amino acid at each position was set to 100%, and other amino acids
715 were adjusted accordingly.
716
717 **Synthesis and screening of individual optimized substrates**
718 ACC-labeled tetrapeptide substrates were synthesized and purified as described elsewhere
719 (Poręba et al., 2014). Substrate hydrolysis at the concentration of 100 µM was carried out for
720 30 min. rCrMCA-II concentration was 2.1 nM. Each experiment was performed in triplicate
721 and the rate of substrate hydrolysis (RFU sec^{-1}) was presented as an average value (S.D. for
722 each substrate hydrolysis was below 15%).
723
724 **Enzyme kinetics**
725 All kinetics experiments were performed using a Gemini XPS (Molecular Devices) plate
726 reader operating in the fluorescence kinetic mode using 96-well plates (Corning®, Costar®).
727 ACC-labeled fluorescent substrates were screened at 355 nm (excitation) and 460 nm
728 (emission) wavelengths under optimal buffer conditions. Buffer was prepared at an ambient
729 temperature and all kinetics measurements were performed at 37°C. The kinetic parameters
730 (k_{cat}, K_M, k_{cat}/K_M) for ACC-labeled substrates were determined using Michaelis-Menten
731 kinetics according to the protocol described by Poreba et al. (2014). All experiments were
732 performed at least in triplicate and the results were presented as average values (S.D. for all
733 tested substrates was below 15%).
734

735 **Synthesis of fluorescent ABPs**

736 Cy5-labeled irreversible ABPs probes for rCrMCA-II were synthesized and purified as
737 described previously (Poreba et al., 2018). In brief, Boc-Ahx-peptide-COOH was synthesized
738 on solid support using 2-chlorotrityl chloride resin and used without further purification. In
739 parallel, the Boc-Arg(Boc)$_2$-AOMK warhead was synthesized through generation of
740 diazomethane and reaction with mixed anhydrides (Boc-Arg(Boc)$_2$-OH → Boc-Arg(Boc)$_2$-
741 CH_2N_2), following by the conversion of the crude product into bromomethyl ketone (Boc-
742 Arg(Boc)$_2$-BMK) and, finally, into acyloxymethyl ketone (Boc-Arg(Boc)$_2$-AOMK). Next, the
743 crude product was de-protected in TFA/DCM mixture, and the NH_2-Arg-AOMK was coupled
744 with Boc-(linker)-peptide-COOH to yield Boc-(linker)-peptide-Arg-AOMK. The product was
745 purified by HPLC, and after Boc de-protection, it was labeled with Cy5 to obtain Cy5-Ahx-
746 peptide-Arg-AOMK. The final products were purified by HPLC, analyzed via HR-MS and
747 HPLC and dissolved in DMSO (10 mM).

748

749 **ABP binding assay**

750 Each reaction contained 0.4 μM rCrMCA-II or rCrMCA-II^{C141A} and indicated concentration
751 of the ABP co-incubated for 5 min. The reaction was stopped by adding SDS sample buffer.
752 Two-hundred ng purified protein was loaded onto an SDS-PAGE gel, which was then
753 scanned at 700 nm using an Odyssey infrared scanner (LI-COR Biosciences). Total protein
754 was visualized after staining with Oriole fluorescent gel stain solution (Bio-Rad) for 1.5-2 h.

755

756 **Genome editing**

757 A Crispr/Cas9 based targeted insertional mutagenesis approach (Picariello et al., 2020) was
758 employed to knockout the *CrMCA-II* gene. A guiding RNA was designed for targeting the
759 exon region flanking the sequences encoding the catalytic dyad to disrupt the *CrMCA-II*.
760 Electroporation was used to introduce a donor DNA comprising of 40 bp flanking sequences,
761 *Hsp70/RBCS2* promoter, *AphVIII* gene, *RBCS2* terminator, and the ribonucleoprotein
762 complex. The resulting transformants were screened with colony PCR and confirmed by
763 immunoblotting with α-CrMCA-II.

764

765 **Genomic DNA isolation**

766 Ten mL of cells grown in TAP were harvested and resuspended in 150 μL H_2O and 300 μL of
767 SDS-EB buffer (2% SDS, 400 mM NaCl, 40 mM EDTA, 100 mM Tris-HCl, pH 8.0). The
768 cell suspension was mixed with 350 μL of phenol:chloroform:isoamyl alcohol (25:24:1) by

769 inverting for few min, which led to the separation of two phases after centrifugation at 2,000 *g*
770 for 5 min. The upper aqueous phase was extracted using 300 µL chloroform:isoamyl alcohol
771 (24:1). The resulting aqueous phase was mixed with two volumes of absolute ethanol and
772 stored at -80°C for 30 min. The genomic DNA was pelleted by centrifugation at 17,000 *g* for
773 10 min and washed twice with 200 µL 70% ethanol. The genomic DNA was then air-dried
774 and dissolved in H_2O.
775
776 **RNA isolation and quantitative PCR (qPCR)**
777 RNA was isolated using Spectrum™ Plant Total RNA Kit (Sigma-Aldrich) according to the
778 manufacturer's instructions. DNAse was added during isolation to remove any remaining
779 genomic DNA. For qPCR analysis, 200 ng of genomic DNA or 12.5 ng complementary DNA
780 of total RNA was used in each reaction. The relative abundances of target genes were
781 calculated using the $2^{-\Delta\Delta Ct}$ method (Livak and Schmittgen, 2001) with RACK1 (Mus et al.,
782 2007) as a reference for normalization. All used primers are listed in Supplemental Table S2.
783
784 **Proteolytic activity assay of Chlamydomonas cell lysates**
785 Ten ml of cells at the density of ~ 1×10^7 cells mL^{-1} were harvested and stored at -80°C.
786 Before extraction, the cells were thawed on ice for 5 min. Each sample was then suspended in
787 150 µL of extraction buffer (50 mM Tris pH 7.5, 25-100 mM NaCl, 1 mM EDTA, 1%
788 glycerol, 1 µM aprotinin, 10 µM pepstatin A, 1 mM PMSF and 2 mM Pefabloc SC) and
789 sonicated for 30 sec by 10-sec pulses, with 5-sec intervals, and the cell debris was pelleted at
790 7,800 *g* for 10 min. The resulting supernatant (cell lysate) was used for the assay. The
791 proteolytic activity was measured in 50 µL extraction buffer supplemented with 0.1%
792 CHAPS, 7.5 mM DTT, 20 mM $CaCl_2$, 50 µM of either VRPR-7-amino-4-methylcoumarin
793 (AMC) or HRTR-ACC, and 1 µL cell lysate. The fluorescent signal was detected by
794 POLARstar Omega Plate Reader (BMG LABTECH).
795
796 **Yeast Two-Hybrid (Y2H) assay**
797 The Y2H experiments were performed as previous described (Zou et al., 2020). The cDNA
798 sequences of CrMCA-II and serpin were cloned into AD or/and BD vector. The BD-CrMCA-
799 II vector was used as a template to construct BD-CrMCA-II-C141A.
800
801 **Chlamydomonas subcellular fractionation**

802 We followed previously published procedures (Norling et al., 1996; Herbik et al., 2002) with
803 some modifications (see Supplemental Figure S13). Briefly, cells were harvested at 4,000 *g*
804 for 5 min and snap-frozen in liquid nitrogen. One to 2 g cells were mixed with 40 mL
805 extraction buffer (250 mM sucrose, 50 mM HEPES pH 7.5, 1 mM EGTA, 1 mM KCl, 0.6%
806 w/v PVPP, 0.1 mM PMSF and 2.5 mM DTT) for 5 min on ice before sonicating twice for 10
807 min on ice. The unbroken cells, chloroplasts and cell debris were removed by centrifugation
808 for 3 min at 1,200 *g*. The first supernatant (S1) was centrifuged for 5 min at 13,000 *g* to
809 remove the pellet containing mainly mitochondria and thylakoids, and to collect the second
810 supernatant (S2) containing low density membranes (LDMs) of Golgi, ER, tonoplast, as well
811 as PM. The S2 was centrifuged for 2 h at 68,000 *g* at 4°C to separate into the LDM-
812 containing pellet (P3) and a supernatant (S3). The P3 was re-suspended in a maximum of 2.5
813 mL re-suspension buffer (250 mM sucrose, 5 mM potassium phosphate pH 7.8, and 5 mM
814 DTT), and the PM vesicles were separated from the endomembranes by two-phase
815 partitioning system. The P3 suspension (2.25 g) was loaded onto an ice-cold polymer mixture
816 (6.75 g) comprised of 6.4% dextran T500, 6.4% polyethyleneglycol (PEG, MW 4,000), 250
817 mM sucrose, 5 mM K-phosphate (pH 7.8) and 5 mM KCl. After centrifugation at 2,000 *g* for
818 10 min, the mixture separated into two phases. The upper PEG phase, containing the PM, was
819 further partitioned against a fresh lower phase to increase the purity of the PM fraction.
820 Subsequently, the PEG and dextran phases were diluted five-fold with the dilution buffer
821 (0.33 M sucrose, 5 mM MOPS pH 7.0, 1 mM EDTA and 2 mM DTT). The PM proteins and
822 the endomembrane proteins were pelleted from the PEG phase and the dextran phase,
823 respectively by centrifugation at 68,000 *g* for 1 h at 4°C. The endomembrane and the PM
824 proteins were re-suspended in dilution buffer for immunoblotting.
825
826 **Protein extraction and immunoblotting**
827 Two ml cells in late log phase (1-2×10^7 cells mL^{-1}) were harvested by centrifugation at 17,
828 000 *g* for 1 min and were snap-frozen in liquid nitrogen. The cell pellet was dissolved in 200
829 µL 1×SDS sample buffer (50 mM Tris-Cl pH 7.5, 100 mM DTT, 2% (w/v) SDS, 0.1% (w/v)
830 Bromophenol Blue, 10% (w/v) glycerol) and incubated at 70°C for 5 min. The samples were
831 vortexed at the highest speed and then centrifuged at 17,000 *g* for 10 min. The resulting
832 supernatant was used for immunoblotting. The α-CrMCA-II was generated by Agrisera using
833 peptide antigen characterized in Supplemental Figure S11A. The α-H^+ ATPase was purchase
834 from Agrisera. Primary antibody dilutions for α-CrMCA-II and α-H^+ ATPase were 1:1,000
835 and 1:5,000, respectively. A secondary anti-rabbit antibody was used at a dilution of 1:10,000.

836

837 **Cell death measurements**

838 Cells in log phase (~5×10^6 cells mL^{-1}) were subjected to HS at 42°C for 1 h and then cooled
839 down to room temperature before treated with Fluorescein Diacetate (FDA, final
840 concentration 2 µg mL^{-1}; Minina et al., 2013). The FDA-treated cells were loaded into
841 hemocytometer and photographed. When excited at 480 nm, living cells appeared green,
842 while dead cells appeared red. Cell death was calculated using the following formula: cell
843 death (%) = dead cells / (dead cells + living cells) *100%.

844

845 **Live imaging of CrMCA-II**

846 The *CrMCA-II* gene was cloned into the MoClo toolkit (Crozet et al., 2018). Subsequently, a
847 plasmid containing *PsaD* promoter, the genomic sequence of *CrMCA-II*, the *mVenus* gene
848 and the *PsaD* terminator was assembled to overexpress CrMCA-II-mVenus. The
849 transformants at log phase were screened and imaged by confocal microscopy (Zeiss LSM
850 780), with the excitation and emission at 514 nm and 540-580 nm, respectively.

851

852 **Fluorescence recovery after photo-bleaching (FRAP)**

853 Due to the high sensitivity to photobleaching at 42°C HS resulting in cell damage, the
854 temperature of HS for the FRAP analysis was reduced to 39°C. The cells were labeled with
855 DiOC6(3) (Invitrogen, final concentration: 0.05 µg/ml) for 1 min at room temperature,
856 followed by 2 washes with fresh TAP medium. The labeled PM was observed by confocal
857 microscopy (LSM 780, Carl Zeiss), with the excitation and emission at 488 nm and 501-570
858 nm, respectively. FRAP analysis was conducted as described (Gutierrez-Beltran et al., 2021),
859 with the following modifications: 60 iterations, 1 sec per frame, and 75% transmittance with
860 the 488-nm laser lines of the argon laser. Pre- and post-bleach scans were performed using the
861 laser power at 0.5% to 2% transmittance for 488 nm and 0% for all other laser lines.

862

863 **Acknowledgements**

864 This work was supported by the Knut and Alice Wallenberg Foundation (grants 2018.0026 to
865 P.V.B. and J.S and 2021.0071 to S.S.) and (grant 2019-01565 to A.N.D.). We would like to
866 thank Dr. Marina Klemenčič (University of Ljubljana) for sharing a plasmid overexpressing
867 CrMCA-II and for fruitful discussions, Dr. George B. Witman and Dr. Yuqing Hou (both
868 from University of Massachusetts Chan Medical School) for advice on genome editing, Dr.

869 Ralph Bock (Max Planck Institute of Molecular Plant Physiology) for sharing algal strain
870 UVM4, and Dr. Anna Maria Eisele (SLU, Uppsala) for fruitful discussions.
871
872 **Author contributions**
873 Y.Z. and P.V.B. designed the study with input from I.S., A.N.D., S.S., M.P., and J.S. Y.Z.,
874 I.S., M.P. and P.V.B. wrote the manuscript. Y.Z., I.S., N.H., A.N.D., A.Å., and L.S.T.
875 performed experiments. M.D. contributed new analytic tools.

References

Becker, B., and Marin, B. (2009). Streptophyte algae and the origin of embryophytes. Ann Bot **103,** 999-1004.

Bemer, K. (1985). Summary of green plant phylogeny and classification. Cladistics **1,** 369-385.

Bollhöner, B., Zhang, B., Stael, S., Denancé, N., Overmyer, K., Goffner, D., Van Breusegem, F., and Tuominen, H. (2013). *Post mortem* function of AtMC9 in xylem vessel elements. New Phytol **200,** 498-510.

Bozhkov, P.V., Suarez, M.F., Filonova, L.H., Daniel, G., Zamyatnin, A.A., Rodriguez-Nieto, S., Zhivotovsky, B., and Smertenko, A. (2005). Cysteine protease mcII-Pa executes programmed cell death during plant embryogenesis. Proc Natl Acad Sci USA **102,** 14463-14468.

Breckenridge, D.G., Nguyen, M., Kuppig, S., Reth, M., and Shore, G.C. (2002). The procaspase-8 isoform, procaspase-8L, recruited to the BAP31 complex at the endoplasmic reticulum. Proc Natl Acad Sci USA **99,** 4331-4336.

Bychkov, E.R., Ahmed, M.R., Gurevich, V.V., Benovic, J.L., and Gurevich, E.V. (2011). Reduced expression of G protein-coupled receptor kinases in schizophrenia but not in schizoaffective disorder. Neurobiol Dis **44,** 248-258.

Cano-Ramirez, D.L., Carmona-Salazar, L., Morales-Cedillo, F., Ramírez-Salcedo, J., Cahoon, E.B., and Gavilanes-Ruíz, M. (2021). Plasma membrane fluidity: An environment thermal detector in plants. Cells **10,** 2778.

Cerretti, D.P., Kozlosky, C.J., Mosley, B., Nelson, N., Ness, K.V., Greenstreet, T.A., March, C.J., Kronheim, S.R., Druck, T., Cannizzaro, L.A., Huebner, K., and Black, R.A. (1992). Molecular cloning of the interleukin-1β converting enzyme. Science **256,** 97-100.

Choi, C.J., and Berges, J.A. (2013). New types of metacaspases in phytoplankton reveal diverse origins of cell death proteases. Cell Death Dis **4,** e490.

Coll, N.S., Smidler, A., Puigvert, M., Popa, C., Valls, M., and Dangl, J.L. (2014). The plant metacaspase AtMC1 in pathogen-triggered programmed cell death and aging: functional linkage with autophagy. Cell Death Differ **21,** 1399-1408.

Coll, N.S., Vercammen, D., Smidler, A., Clover, C., Van Breusegem, F., Dangl, J.L., and Epple, P. (2010). *Arabidopsis* type I metacaspases control cell death. Science **330,** 1393-1397.

Conchou, L., Doumèche, B., Galisson, F., Violot, S., Dugelay, C., Diesis, E., Page, A., Bienvenu, A.-L., Picot, S., Aghajari, N., and Ballut, L. (2022). Structural and molecular determinants of Candida glabrata metacaspase maturation and activation by calcium. Commun Biol **5,** 1158.

Crozet, P., Navarro, F.J., Willmund, F., Mehrshahi, P., Bakowski, K., and et al. (2018). Birth of a photosynthetic chassis: A MoClo toolkit enabling synthetic biology in the microalga *Chlamydomonas reinhardtii*. Acs Synth Biol **7,** 2074-2086.

Desai, A.J., and Miller, L.J. (2018). Changes in the plasma membrane in metabolic disease: impact of the membrane environment on G protein-coupled receptor structure and function. Br J Pharmacol **175,** 4009-4025.

Feig, C., Tchikov, V., Schütze, S., and Peter, M.E. (2007). Palmitoylation of CD95 facilitates formation of SDS-stable receptor aggregates that initiate apoptosis signaling. EMBO J **26,** 221-231.

Finlay, D., and Vuori, K. (2007). Novel noncatalytic role for caspase-8 in promoting Src-mediated adhesion and Erk signaling in neuroblastoma cells. Cancer Res **67,** 11704-11711.

926 **Graff van Creveld, S., Ben-Dor, S., Mizrachi, A., Alcolombri, U., Hopes, A., Mock, T.,**
927 **Rosenwasser, S., and Vardi, A.** (2021). Biochemical characterization of a novel
928 redox-regulated metacaspase in a marine diatom. Front Microbiol **12**.
929 **Guihur, A., Rebeaud, M.E., and Goloubinoff, P.** (2022). How do plants feel the heat and
930 survive? Trends Biochem Sci **47,** 824-838.
931 **Gutierrez-Beltran, E., Elander, P.H., Dalman, K., Dayhoff II, G.W., Moschou, P.N.,**
932 **Uversky, V.N., Crespo, J.L., and Bozhkov, P.V.** (2021). Tudor staphylococcal
933 nuclease is a docking platform for stress granule components and is essential for
934 SnRK1 activation in Arabidopsis. EMBO J **40,** e105043.
935 **Gutman, B.L., and Niyogi, K.K.** (2004). Chlamydomonas and Arabidopsis. A dynamic duo.
936 Plant Physiol **135,** 607-610.
937 **Haire, T.C., Bell, C., Cutshaw, K., Swiger, B., Winkelmann, K., and Palmer, A.G.**
938 (2018). Robust microplate-based methods for culturing and in vivo phenotypic
939 screening of *Chlamydomonas reinhardtii*. Front Plant Sci **9**.
940 **Hallgren, J., Tsirigos, K.D., Pedersen, M.D., Almagro Armenteros, J.J., Marcatili, P.,**
941 **Nielsen, H., Krogh, A., and Winther, O.** (2022). DeepTMHMM predicts alpha and
942 beta transmembrane proteins using deep neural networks. bioRxiv**,**
943 2022.2004.2008.487609.
944 **Hander, T., Fernández-Fernández, Á.D., Kumpf, R.P., Willems, P., Schatowitz, H.,**
945 **Rombaut, D., Staes, A., Nolf, J., Pottie, R., Yao, P., Gonçalves, A., Pavie, B.,**
946 **Boller, T., Gevaert, K., Van Breusegem, F., Bartels, S., and Stael, S.** (2019).
947 Damage on plants activates Ca^{2+}-dependent metacaspases for release of
948 immunomodulatory peptides. Science **363,** eaar7486.
949 **Herbik, A., Haebel, S., and Buckhout, T.J.** (2002). Is a ferroxidase involved in the high-
950 affinity iron uptake in *Chlamydomonas reinhardtii*? Plant Soil **241,** 1-10.
951 **Hill, S.M., Hao, X.X., Liu, B.D., and Nystrom, T.** (2014). Life-span extension by a
952 metacaspase in the yeast Saccharomyces cerevisiae. Science **344,** 1389-1392.
953 **Hoebeeck, J., Speleman, F., and Vandesompele, J.** (2007). Real-time quantitative PCR as
954 an alternative to southern blot or fluorescence in situ hybridization for detection of
955 gene copy number changes. In Methods Mol Biol (Protocols for Nucleic Acid
956 Analysis by Nonradioactive Probes), E. Hilario and J. Mackay, eds (Totowa, NJ:
957 Humana Press), pp. 205-226.
958 **Horn, A., and Jaiswal, J.K.** (2019). Structural and signaling role of lipids in plasma
959 membrane repair. In Curr Top Membr, L.O. Andrade, ed (Academic Press), pp. 67-98.
960 **Horváth, I., Multhoff, G., Sonnleitner, A., and Vígh, L.** (2008). Membrane-associated
961 stress proteins: More than simply chaperones. Biochim Biophys Acta Biomembr **1778,**
962 1653-1664.
963 **Huh, S.U.** (2022). Evolutionary diversity and function of metacaspases in plants: Similar to
964 but not caspases. Int J Mol Sci **23,** 4588.
965 **Jaillais, Y., and Ott, T.** (2019). The nanoscale organization of the plasma membrane and its
966 importance in signaling: A proteolipid perspective. Plant Physiol **182,** 1682-1696.
967 **Julien, O., and Wells, J.A.** (2017). Caspases and their substrates. Cell Death Differ **24,** 1380-
968 1389.
969 **Kato, D., Boatright, K.M., Berger, A.B., Nazif, T., Blum, G., Ryan, C., Chehade, K.A.H.,**
970 **Salvesen, G.S., and Bogyo, M.** (2005). Activity-based probes that target diverse
971 cysteine protease families. Nat Chem Biol **1,** 33-38.
972 **Kesavardhana, S., Malireddi, R.K.S., and Kanneganti, T.-D.** (2020). Caspases in cell
973 death, inflammation, and pyroptosis. Annu Rev Immunol **38,** 567-595.
974 **Klemenčič, M., and Funk, C.** (2018). Structural and functional diversity of caspase
975 homologues in non-metazoan organisms. Protoplasma **255,** 387-397.

976 **Klemenčič, M., and Funk, C.** (2019). Evolution and structural diversity of metacaspases. J
977 Exp Bot **70,** 2039-2047.
978 **Kumar, S., Stecher, G., Li, M., Knyaz, C., and Tamura, K.** (2018). MEGA X: Molecular
979 evolutionary genetics analysis across computing platforms. Mol Biol Evol **35,** 1547-
980 1549.
981 **La, S.R., Ndhlovu, A., and Durand, P.M.** (2022). The ancient origins of death domains
982 support the 'original sin' hypothesis for the evolution of programmed cell death. J Mol
983 Evol **90,** 95-113.
984 **Lam, E., and Zhang, Y.** (2012). Regulating the reapers: activating metacaspases for
985 programmed cell death. Trends in Plant Sci **17,** 487-494.
986 **Lee, R.E.C., Brunette, S., Puente, L.G., and Megeney, L.A.** (2010). Metacaspase Yca1 is
987 required for clearance of insoluble protein aggregates. Proc Natl Acad Sci USA **107,**
988 13348-13353.
989 **Li, Y., Xue, J., Wang, F.-Z., Huang, X., Gong, B.-Q., Tao, Y., Shen, W., Tao, K., Yao, N.,**
990 **Xiao, S., Zhou, J.-M., and Li, J.-F.** (2022). Plasma membrane-nucleo-cytoplasmic
991 coordination of a receptor-like cytoplasmic kinase promotes EDS1-dependent plant
992 immunity. Nat Plants **8,** 802-816.
993 **Livak, K.J., and Schmittgen, T.D.** (2001). Analysis of relative gene expression data using
994 real-time quantitative PCR and the $2^{-\Delta\Delta CT}$ method. Methods **25,** 402-408.
995 **Long, H., Zhang, F., Xu, N., Liu, G., Diener, D.R., Rosenbaum, J.L., and Huang, K.**
996 (2016). Comparative analysis of ciliary membranes and ectosomes. Curr Biol **26,**
997 3327-3335.
998 **MacKenzie, S.H., and Clark, A.C.** (2012). Death by caspase dimerization. In Adv Exp Med
999 Biol (Protein Dimerization and Oligomerization in Biology), J.M. Matthews, ed (New
1000 York, NY: Springer New York), pp. 55-73.
1001 **McConnell, E.W., Werth, E.G., and Hicks, L.M.** (2018). The phosphorylated redox
1002 proteome of *Chlamydomonas reinhardtii*: Revealing novel means for regulation of
1003 protein structure and function. Redox Biol **17,** 35-46.
1004 **McLuskey, K., and Mottram, Jeremy C.** (2015). Comparative structural analysis of the
1005 caspase family with other clan CD cysteine peptidases. Biochem **466,** 219-232.
1006 **McLuskey, K., Rudolf, J., Proto, W.R., Isaacs, N.W., Coombs, G.H., Moss, C.X., and**
1007 **Mottram, J.C.** (2012). Crystal structure of a *Trypanosoma brucei* metacaspase. Proc
1008 Natl Acad Sci USA **109,** 7469-7474.
1009 **Merchant, S.S., Prochnik, S.E., Vallon, O., Harris, E.H., Karpowicz, S.J., and et, a.l.**
1010 (2007). The *Chlamydomonas* genome reveals the evolution of key animal and plant
1011 functions. Science **318,** 245-250.
1012 **Minina, E.A., Coll, N.S., Tuominen, H., and Bozhkov, P.V.** (2017). Metacaspases versus
1013 caspases in development and cell fate regulation. Cell Death Differ **24,** 1314-1325.
1014 **Minina, E.A., Filonova, L.H., Sanchez-Vera, V., Suarez, M.F., Daniel, G., and Bozhkov,**
1015 **P.V.** (2013). Detection and measurement of necrosis in plants. In Methods Protoc
1016 (Necrosis), K. McCall and C. Klein, eds (Totowa, NJ: Humana Press), pp. 229-248.
1017 **Minina, E.A., Staal, J., Alvarez, V.E., Berges, J.A., Berman-Frank, I., and et, a.l.** (2020).
1018 Classification and nomenclature of metacaspases and paracaspases: No more
1019 confusion with caspases. Mol Cell **77,** 927-929.
1020 **Mittler, R., Finka, A., and Goloubinoff, P.** (2012). How do plants feel the heat? Trends
1021 Biochem Sci **37,** 118-125.
1022 **Morris, J.L., Puttick, M.N., Clark, J.W., Edwards, D., Kenrick, P., Pressel, S., Wellman,**
1023 **C.H., Yang, Z., Schneider, H., and Donoghue, P.C.J.** (2018). The timescale of early
1024 land plant evolution. Proc Natl Acad Sci USA **115,** E2274-E2283.

1025 **Mus, F., Dubini, A., Seibert, M., Posewitz, M.C., and Grossman, A.R.** (2007). Anaerobic
1026 acclimation in *Chlamydomonas reinhardtii*: anoxic gene expression, hydrogenase
1027 induction, and metabolic pathways. J Biol Chem **282,** 25475-25486.
1028 **Neupert, J., Karcher, D., and Bock, R.** (2009). Generation of *Chlamydomonas* strains that
1029 efficiently express nuclear transgenes. Plant J **57,** 1140-1150.
1030 **Ning, W., Jiang, P., Guo, Y., Wang, C., Tan, X., Zhang, W., Peng, D., and Xue, Y.**
1031 (2020). GPS-Palm: a deep learning-based graphic presentation system for the
1032 prediction of S-palmitoylation sites in proteins. Brief Bioinformatics **22,** 1836-1847.
1033 **Niu, Y., and Xiang, Y.** (2018). An overview of biomembrane functions in plant responses to
1034 high-temperature stress. Front Plant Sci **9**.
1035 **Nordzieke, D.E., and Medraño-Fernandez, I.** (2018). The plasma membrane: A platform
1036 for intra- and intercellular redox signaling. Antioxidants **7,** 168.
1037 **Norling, B., Nurani, G., and Franzén, L.-G.** (1996). Characterisation of the H^+-ATPase in
1038 plasma membranes isolated from the green alga *Chlamydomonas reinhardtii*. Physiol
1039 Plant **97,** 445-453.
1040 **Pérez-Pérez, M.E., Mauriès, A., Maes, A., Tourasse, N.J., Hamon, M., Lemaire, S.D.,**
1041 **and Marchand, C.H.** (2017). The deep thioredoxome in *Chlamydomonas reinhardtii*:
1042 New insights into redox regulation. Mol Plant **10,** 1107-1125.
1043 **Picariello, T., Hou, Y., Kubo, T., McNeill, N.A., Yanagisawa, H.-a., Oda, T., and**
1044 **Witman, G.B.** (2020). TIM, a targeted insertional mutagenesis method utilizing
1045 CRISPR/Cas9 in *Chlamydomonas reinhardtii*. PloS One **15,** e0232594.
1046 **Poreba, M., Salvesen, G.S., and Drag, M.** (2017). Synthesis of a HyCoSuL peptide
1047 substrate library to dissect protease substrate specificity. Nat Protoc **12,** 2189-2214.
1048 **Poreba, M., Rut, W., Vizovisek, M., Groborz, K., Kasperkiewicz, P., Finlay, D., Vuori,**
1049 **K., Turk, D., Turk, B., Salvesen, G.S., and Drag, M.** (2018). Selective imaging of
1050 cathepsin L in breast cancer by fluorescent activity-based probes. Chem **9,** 2113-2129.
1051 **Poręba, M., Szalek, A., Kasperkiewicz, P., and Drąg, M.** (2014). Positional scanning
1052 substrate combinatorial library (PS-SCL) approach to define caspase substrate
1053 specificity In Methods Protoc (Caspases,Paracaspases, and Metacaspases), P. V.
1054 Bozhkov and G. Salvesen, eds (New York, NY: Springer New York), pp. 41-59.
1055 **Pozza, A., Giraud, F., Cece, Q., Casiraghi, M., Point, E., Damian, M., Le Bon, C.,**
1056 **Moncoq, K., Banères, J.-L., Lescop, E., and Catoire, L.J.** (2022). Exploration of
1057 the dynamic interplay between lipids and membrane proteins by hydrostatic pressure.
1058 Nat Commun **13,** 1780.
1059 **Proto, W.R., Castanys-Munoz, E., Black, A., Tetley, L., Moss, C.X., Juliano, L., Coombs,**
1060 **G.H., and Mottram, J.C.** (2011). Trypanosoma brucei metacaspase 4 is a
1061 pseudopeptidase and a virulence factor. J Biol Chem **286,** 39914-39925.
1062 **Ross, C., Chan, A.H., Pein, J.B.v., Maddugoda, M.P., Boucher, D., and Schroder, K.**
1063 (2022). Inflammatory caspases: Toward a unified model for caspase activation by
1064 inflammasomes. Annu Rev Immunol **40,** 249-269.
1065 **Sabljić, I., Zou, Y., Klemenčič, M., Funk, C., Ståhlberg, J., and Bozhkov, P.** (2022).
1066 Expression andpurification of the type II metacaspase from a unicellular green alga
1067 *Chlamydomonas reinhardtii*. In Methods Protoc (Plant Proteases and Plant Cell
1068 Death), M. Klemenčič, S. Stael, and P.F. Huesgen, eds (New York, NY: Springer US),
1069 pp. 13-20.
1070 **Saidi, Y., Finka, A., Muriset, M., Bromberg, Z., Weiss, Y.G., Maathuis, F.J.M., and**
1071 **Goloubinoff, P.** (2009). The heat shock response in moss plants is regulated by
1072 specific calcium-permeable channels in the plasma membrane Plant Cell **21,** 2829-
1073 2843.

1074 **Salguero-Linares, J., and Coll, N.S.** (2019). Plant proteases in the control of the
1075 hypersensitive response. J Exp Bot **70,** 2087-2095.
1076 **Schneider-Poetsch, T., Ju, J., Eyler, D.E., Dang, Y., Bhat, S., Merrick, W.C., Green, R.,**
1077 **Shen, B., and Liu, J.O.** (2010). Inhibition of eukaryotic translation elongation by
1078 cycloheximide and lactimidomycin. Nat Chem Biol **6,** 209-217.
1079 **Schroda, M., Hemme, D., and Mühlhaus, T.** (2015). The *Chlamydomonas* heat stress
1080 response. Plant J. **82,** 466-480.
1081 **Shen, W., Liu, J., and Li, J.-F.** (2019). Type-II metacaspases mediate the processing of plant
1082 elicitor peptides in *Arabidopsis*. Mol Plant **12,** 1524-1533.
1083 **Shuba, Y.M.** (2021). Beyond neuronal heat sensing: Diversity of trpv1 heat-capsaicin
1084 receptor-channel functions. Front Cell Neurosci **14**.
1085 **Stael, S., Wurzinger, B., Mair, A., Mehlmer, N., Vothknecht, U.C., and Teige, M.** (2011).
1086 Plant organellar calcium signalling: an emerging field. J Exp Bot **63,** 1525-1542.
1087 **Stael, S., Sabljić, I., Audenaert, D., Andersson, T., Tsiatsiani, L., Kumpf, R.P., Vidal-**
1088 **Albalat, A., Lindgren, C., Vercammen, D., Jacques, S., Nguyen, L., Njo, M.,**
1089 **Fernández-Fernández, Á.D., Beunens, T., Timmerman, E., Gevaert, K.,**
1090 **Ståhlberg, J., Bozhkov, P.V., Linusson, A., Beeckman, T., and Van Breusegem, F.**
1091 (2023). Structure-function analysis of a Ca^{2+}-independent metacaspase reveals a novel
1092 proteolytic pathway for lateral root emergence. Proc Natl Acad Sci USA **120,**
1093 e2303480120.
1094 **Stennicke, H.R., and Salvesan, G.S.** (1997). Biochemical characteristics of caspases-3, -6, -
1095 7, and -8. J Biol Chem **272,** 25719-25723.
1096 **Sundström, J.F., Vaculova, A., Smertenko, A.P., Savenkov, E.I., Golovko, A., Minina,**
1097 **E., Tiwari, B.S., Rodriguez-Nieto, S., Zamyatnin Jr, A.A., Välineva, T.,**
1098 **Saarikettu, J., Frilander, M.J., Suarez, M.F., Zavialov, A., Ståhl, U., Hussey, P.J.,**
1099 **Silvennoinen, O., Sundberg, E., Zhivotovsky, B., and Bozhkov, P.V.** (2009). Tudor
1100 staphylococcal nuclease is an evolutionarily conserved component of the programmed
1101 cell death degradome. Nat Cell Biol **11,** 1347-1354.
1102 **Tekpli, X., Holme, J.A., Sergent, O., and Lagadic-Gossmann, D.** (2013). Role for
1103 membrane remodeling in cell death: Implication for health and disease. Toxicology
1104 **304,** 141-157.
1105 **Thornberry, N.A., Bull, H.G., Calaycay, J.R., Chapman, K.T., Howard, A.D., Kostura,**
1106 **M.J., Miller, D.K., Molineaux, S.M., Weidner, J.R., Aunins, J., Elliston, K.O.,**
1107 **Ayala, J.M., Casano, F.J., Chin, J., Ding, G.J.F., Egger, L.A., Gaffney, E.P.,**
1108 **Limjuco, G., Palyha, O.C., Raju, S.M., Rolando, A.M., Salley, J.P., Yamin, T.-T.,**
1109 **Lee, T.D., Shively, J.E., MacCross, M., Mumford, R.A., Schmidt, J.A., and Tocci,**
1110 **M.J.** (1992). A novel heterodimeric cysteine protease is required for interleukin-1β
1111 processing in monocytes. Nature **356,** 768-774.
1112 **Tsiatsiani, L., Van Breusegem, F., Gallois, P., Zavialov, A., Lam, E., and Bozhkov, P.V.**
1113 (2011). Metacaspases. Cell Death Differ **18,** 1279-1288.
1114 **Tsiatsiani, L., Timmerman, E., De Bock, P.-J., Vercammen, D., Stael, S., van de Cotte,**
1115 **B., Staes, A., Goethals, M., Beunens, T., Van Damme, P., Gevaert, K., and Van**
1116 **Breusegem, F.** (2013). The *Arabidopsis* METACASPASE9 degradome. The Plant
1117 Cell **25,** 2831-2847.
1118 **Uren, A.G., O'Rourke, K., Aravind, L., Pisabarro, M.T., Seshagiri, S., Koonin, E.V., and**
1119 **Dixit, V.M.** (2000). Identification of paracaspases and metacaspases: Two ancient
1120 families of caspase-like proteins, one of which plays a key role in MALT lymphoma.
1121 Mol Cell **6,** 961-967.
1122 **Van Opdenbosch, N., and Lamkanfi, M.** (2019). Caspases in cell death, inflammation, and
1123 disease. Immunity **50,** 1352-1364.

1124 **Vercammen, D., van de Cotte, B., De Jaeger, G., Eeckhout, D., Casteels, P., Vandepoele,**
1125 **K., Vandenberghe, I., Van Beeumen, J., Inze, D., and Van Breusegem, F.** (2004).
1126 Type II metacaspases Atmc4 and Atmc9 of *Arabidopsis thaliana* cleave substrates
1127 after arginine and lysine. J Biol Chem **279,** 45329-45336.
1128 **Vercammen, D., Belenghi, B., van de Cotte, B., Beunens, T., Gavigan, J.-A., De Rycke,**
1129 **R., Brackenier, A., Inzé, D., Harris, J.L., and Van Breusegem, F.** (2006). Serpin1
1130 of *Arabidopsis thaliana* is a suicide inhibitor for metacaspase 9. J Mol Biol **364,** 625-
1131 636.
1132 **Wang, S., Xue, M., He, C., Shen, D., Jiang, C., Zhao, H., and Niu, D.** (2021). AtMC1
1133 associates with LSM4 to regulate plant immunity through modulating pre-mRNA
1134 splicing. Mol Plant Microbe Interact **34,** 1423-1432.
1135 **Watanabe, N., and Lam, E.** (2011). Calcium-dependent activation and autolysis of
1136 *Arabidopsis* metacaspase 2d. J Biol Chem **286,** 10027-10040.
1137 **Wong, A.H.-H., Yan, C., and Shi, Y.** (2012). Crystal structure of the yeast metacaspase
1138 Yca1. J Biol Chem **87,** 29251–29259.
1139 **Yuan, J., Shaham, S., Ledoux, S., Ellis, H.M., and Horvitz, H.R.** (1993). The C. elegans
1140 cell death gene *ced-3* encodes a protein similar to mammalian interleukin-1β-
1141 converting enzyme. Cell **75,** 641-652.
1142 **Zhang, N., Mattoon, E.M., McHargue, W., Venn, B., Zimmer, D., Pecani, K., Jeong, J.,**
1143 **Anderson, C.M., Chen, C., Berry, J.C., Xia, M., Tzeng, S.-C., Becker, E.,**
1144 **Pazouki, L., Evans, B., Cross, F., Cheng, J., Czymmek, K.J., Schroda, M.,**
1145 **Mühlhaus, T., and Zhang, R.** (2022). Systems-wide analysis revealed shared and
1146 unique responses to moderate and acute high temperatures in the green alga
1147 *Chlamydomonas reinhardtii*. Commun Biol **5,** 460.
1148 **Zhang, Y., Launay, H., Schramm, A., Lebrun, R., and Gontero, B.** (2018). Exploring
1149 intrinsically disordered proteins in *Chlamydomonas reinhardtii*. Sci Rep **8,** 6805.
1150 **Zhu, P., Yu, X.H., Wang, C., Zhang, Q., Liu, W., McSweeney, S., Shanklin, J., Lam, E.,**
1151 **and Liu, Q.** (2020). Structural basis for Ca^{2+}-dependent activation of a plant
1152 metacaspase. Nat Commun **11,** 1-38.
1153 **Zou, Y., Li, R., and Baldwin, I.T.** (2020). ZEITLUPE is required for shade avoidance in the
1154 wild tobacco *Nicotiana attenuata*. J Integr Plant Biol **62,** 1341-1351.
1155
1156

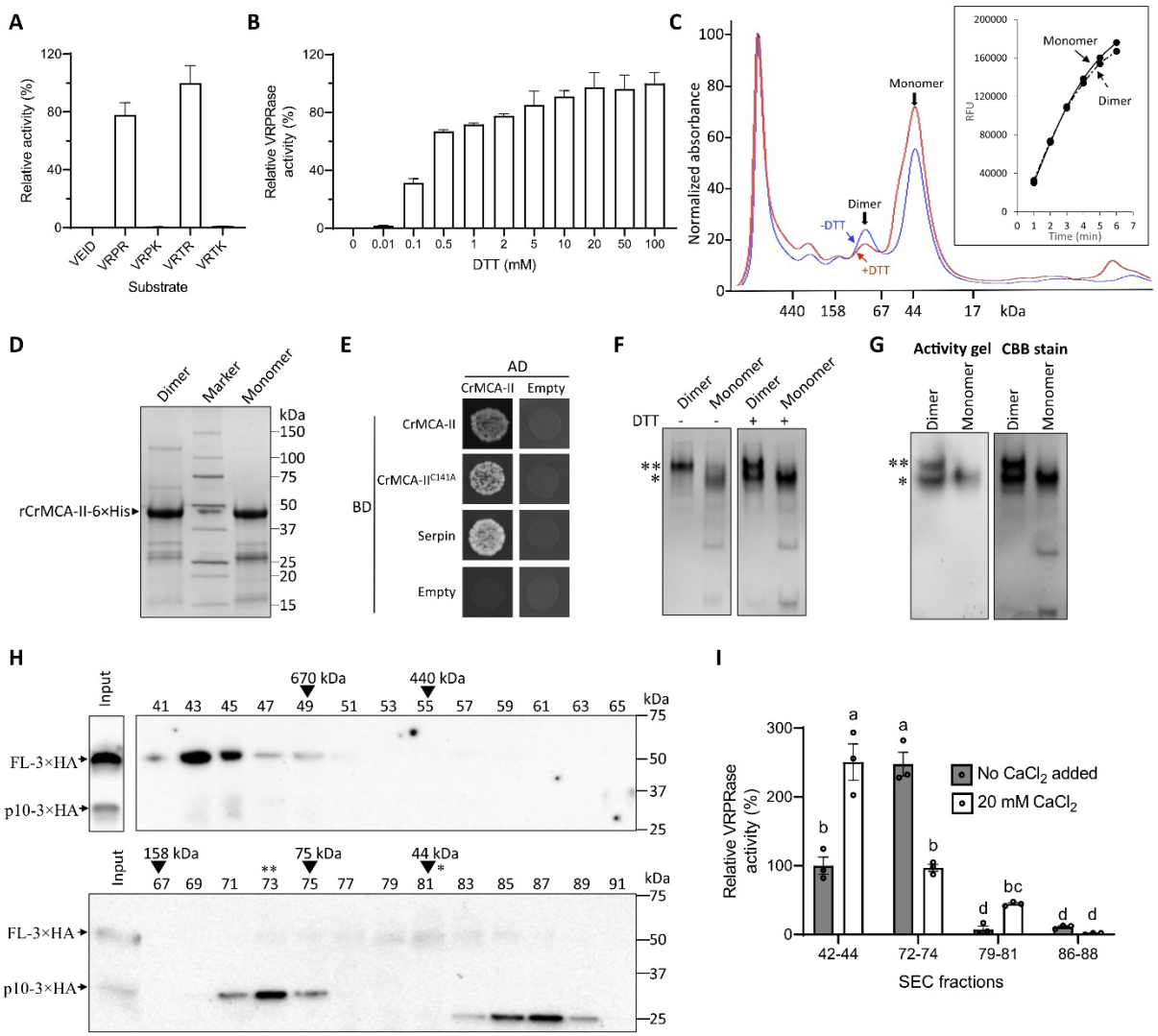

Figure 1 CrMCA-II is a redox-dependent arginine-specific protease prone to oligomerization. **A.** Proteolytic activity of rCrMCA-II against AMC-conjugated tetrapeptide substrates with Arg, Lys, or Asp at the P1 position, relative to Ac-VRTR-AMC, under optimal buffer conditions (50 mM Tris pH 7.5, 25 mM NaCl, 20 mM $CaCl_2$, 0.1% CHAPS and 7.5 mM DTT). **B.** Proteolytic activity of rCrMCA-II, as affected by DTT concentration, relative to 100 mM DTT, under optimal buffer conditions, with 50 µM Ac-VRPR-AMC as a substrate. **C.** The size exclusion chromatography (SEC) of rCrMCA-II in the presence and absence of 1 mM DTT. The insert shows proteolytic activity (relative fluorescence units, RFU) of monomeric and dimeric forms of rCrCMA-II separated in the absence of DTT against Ac-VRPR-AMC under optimal buffer conditions. **D.** SDS-PAGE analysis of dimer- and monomer-containing fractions from **C** separated without DTT. **E.** The Y2H assay of CrMCA-II self-interaction and interaction between wild type protease and its catalytically inactive mutant CrMCA-II^{C141A}. Interaction between CrMCA-II and serpin, an *in vivo* inhibitor of plant metacaspases, was used as a positive control. **F.** Native PAGE of monomeric and

dimeric forms of rCrMCA-II with (+) or without (-) DTT (7.5 mM). **G.** An in-gel proteolytic activity assay of monomeric and dimeric forms of CrMCA-II using native PAGE under optimal buffer conditions, with 50 μM Ac-VRPR-AMC as a substrate. * and ** in **F** and **G** indicate positions of monomer and dimer, respectively. CBB, Coomassie brilliant blue. **H.** Immunoblot analysis of total protein extracts isolated from Chlamydomonas *crmca-ii* mutant strain expressing CrMCA-II-3×HA (see Fig. 3) and fractionated by SEC. Uneven fractions from 41 to 91 were separated by SDS-PAGE and analyzed with **α**-HA. The fractions containing protein standards with indicated molecular masses are marked with arrowheads. Based on the calibration curve, the predicted average molecular masses of proteins in fractions 43, 73 and 87 are 1185 kDa, 88.5 kDa and 26.4 kDa, respectively. The theoretical masses of CrMCA-II-3×HA zymogen (full-length monomer, FL-3×HA) and C-terminal p10 fragment (p10-3×HA; generated via auto-cleavage after Arg190) are 46.1 kDa and 25.9 kDa, respectively. The fractions enriched for CrMCA-II-3×HA monomer and dimer are denoted by * and **, respectively. **I.** The peptide (Ac-VRPR-AMC) cleavage assay of a subset of SEC fractions from **H** and enriched for megadalton CrMCA-II-3×HA assemblies (fractions 42-44), dimer (fractions 72-74), monomer (fractions 79-81), and a fragment smaller than p10 (fractions 86-88). The assay was performed under optimal buffer conditions, with or without addition of 20 mM $CaCl_2$. Note the presence of a basal level of cell-derived Ca^{2+} in the assay. Data in **A, B,** and **I** represent the means ± SEM of triplicate measurements. Different letters indicate significant differences at $p < 0.05$ (a two-way ANOVA with Tukey's honest significant difference test).

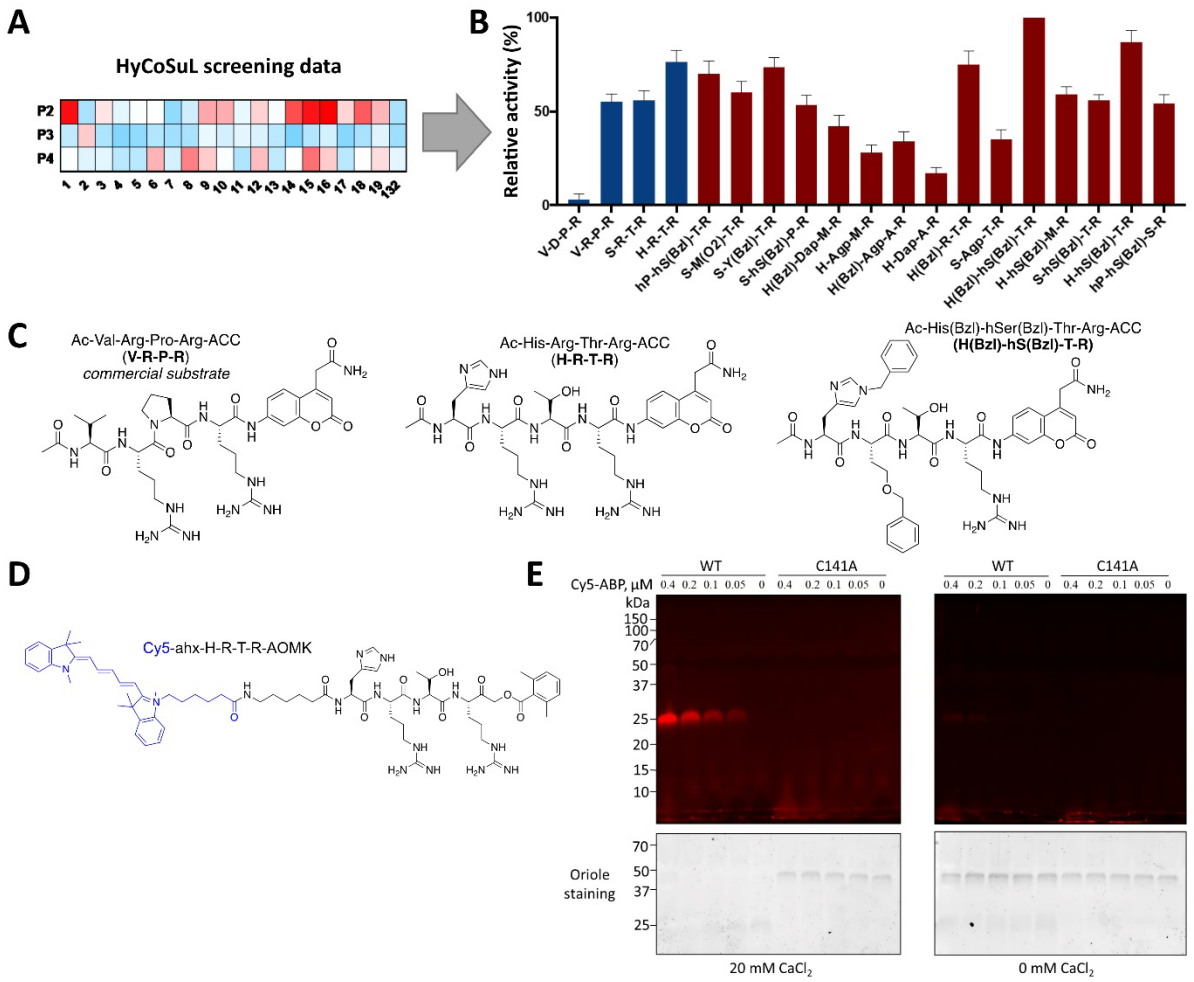

Figure 2 A chemical toolbox for CrMCA-II. **A.** HyCoSuL screening data were used to extract optimal peptide sequences for CrMCA-II substrates and activity-based probes. **B.** Proteolytic activity of rCrMCA-II against individual fluorescent substrates containing natural (blue bars) and unnatural amino acids (red bars). Data represent the means ± SEM of triplicate measurements. **C.** The structures of rCrMCA-II substrates: Ac-VRPR-ACC (commercially available as Ac-VRPR-AMC), Ac-HRTR-ACC (most preferred with natural amino acids), and Ac-H(Bzl)-hS(Bzl)-TR-ACC (most preferred with unnatural amino acids). **D.** The structure of Cy5-labelled covalent activity-based probe (Cy5-ABP) with HRTR peptide motif and AOMK electrophilic warhead. **E.** The binding of Cy5-ABP at different concentrations to 0.4 μM wild-type (WT) rCrMCA-II or its catalytically inactive mutant (C141A) under optimal buffer conditions, in the absence or presence of 20 mM $CaCl_2$, visualized after SDS-PAGE.

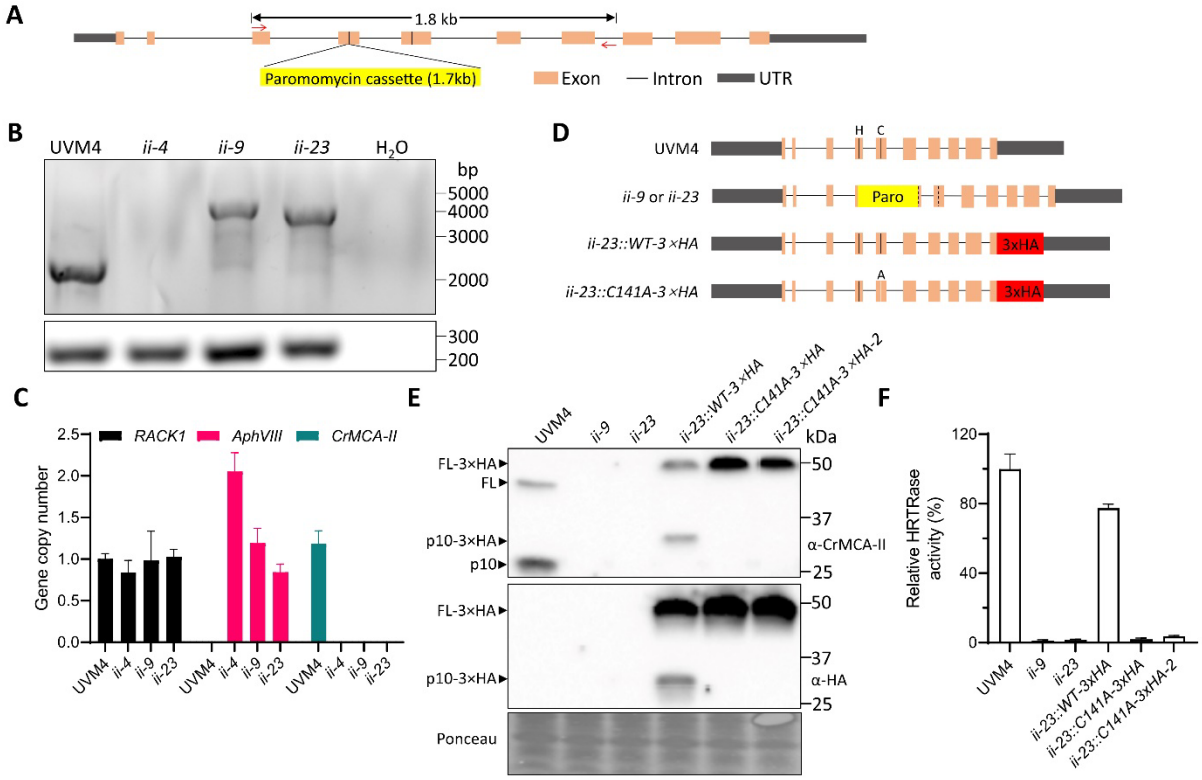

Figure 3 The generation of *crmca-ii* mutant and complementation strains in UVM4 background. **A.** Schematic illustration of the editing site of *CrMCA-II* gene and a pair of primers (red arrows) used for PCR analysis. The vertical lines in exons 4 and 5 indicate the position of a catalytic dyad of His87 and Cys141. **B.** PCR test using the primer pair depicted in **A** with genomic DNA as a template. Distilled water was used as a negative control. Bottom panel shows PCR product of *RACK1* amplification (positive control). *ii-4*, *ii-9* and *ii-23* are presumed mutant strains. **C.** Real-time quantitative PCR (RT-qPCR) analysis of *RACK1*, *AphvIII* and *CrMCA-II* genes using genomic DNA as a template to evaluate genome insertion events. Data represent the means ± SEM of triplicate measurements. Paro, paromomycin resistance cassette. **D.** Schematic illustration of *CrMCA-II* gene structure in the generated strains. The vertical lines indicate position of a catalytic dyad of His87 (H) and Cys141 (C), and a substitution of Cys141 for Ala (A) in strains complemented with a catalytically inactive mutant. The dashed vertical lines corresponding to a catalytic dyad indicate abolished transcription in the mutant strains. **E.** Immunoblot analysis of CrMCA-II in UVM4, *CrMCA-II* mutant (*ii-9* and *ii-23*), and complementation strains (one *ii-23::WT-3×HA* strain and two *ii-23::C141A-3×HA* strains) using **α**-CrMCA-II and **α**-HA. Ponceau staining was used as a loading control. **F.** The peptide (Ac-HRTR-ACC) cleavage assay of cell lysates (total protein extracts) from the same strains as in **E.** Data represent the means ± SEM from three independent biological replicates.

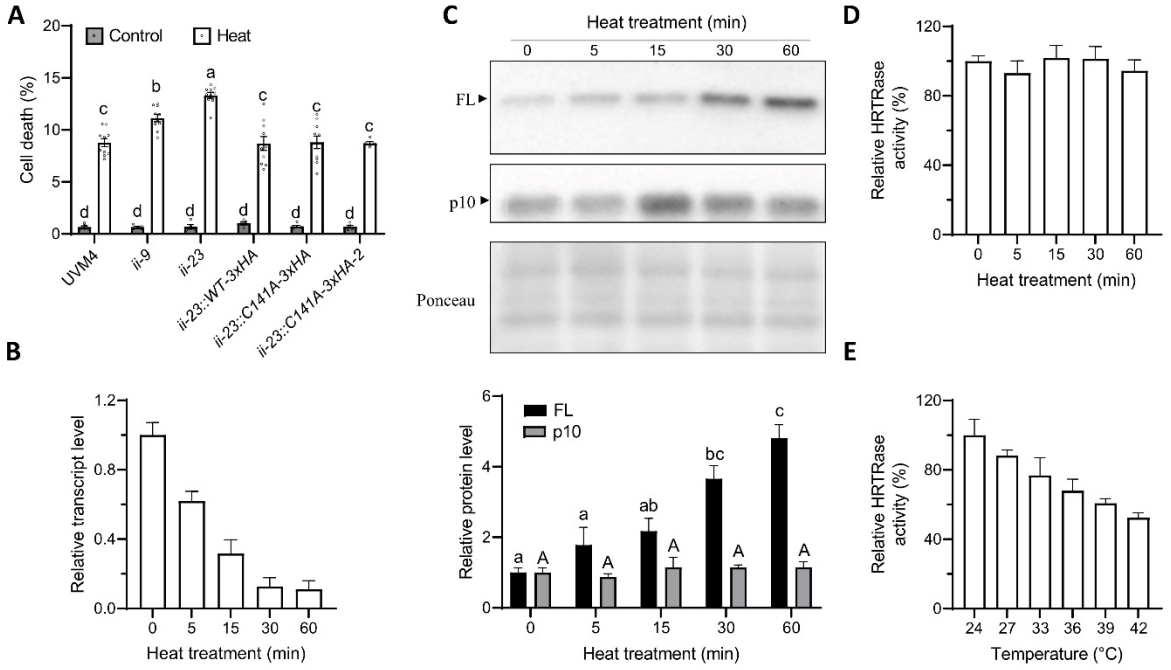

Figure 4 CrMCA-II plays a cytoprotective role during HS. **A.** The frequency of cell death in the UVM4, mutant and complementation strains growing under control conditions (23°C; Control) or subjected to 60-min HS at 42°C (Heat), as determined by FDA staining. **B.** The relative transcript levels of *CrMCA-II* in the UVM4 strain at 0, 5, 15, 30 and 60 min HS at 42°C determined by RT-qPCR. The transcript level at 0 min was set to 1. **C.** Immunoblot analysis of full-length (FL) and p10 fragment of CrMCA-II in total protein extracts isolated from the UVM4 strain at 0, 5, 15, 30, and 60 min of HS at 42 °C. The chart shows relative levels of the FL and p10 based on densitometry analysis of the corresponding bands. The levels of FL and p10 at 0 min were set to 1, respectively. Ponceau staining was used as a loading control. **D.** The relative HRTRase activity of cell lysates isolated from the UVM4 strain at 0, 5, 15, 30, and 60 min of HS at 42°C. **E.** The relative HRTRase activity of rCrMCA-II pre-treated for 5 min at different temperatures in Ca^{2+}- and DTT-free buffer (non-permissive conditions) before activity measurements under optimal buffer conditions. The data shown on charts **A** and **C** were analyzed using a two-way ANOVA with Tukey's honest significant difference test. Different letters indicate significant differences at $p < 0.05$. Data on charts **A** and **C** represent the means ± SEM from three independent biological replicates, with each replicate in case of **A** including triplicate measurements. Different letters indicate significant differences at $p < 0.05$ (a two-way ANOVA with Tukey's honest significant difference test). Data in **B**, **D** and **E** show the means ± SEM of one representative experiment with triplicate measurements.

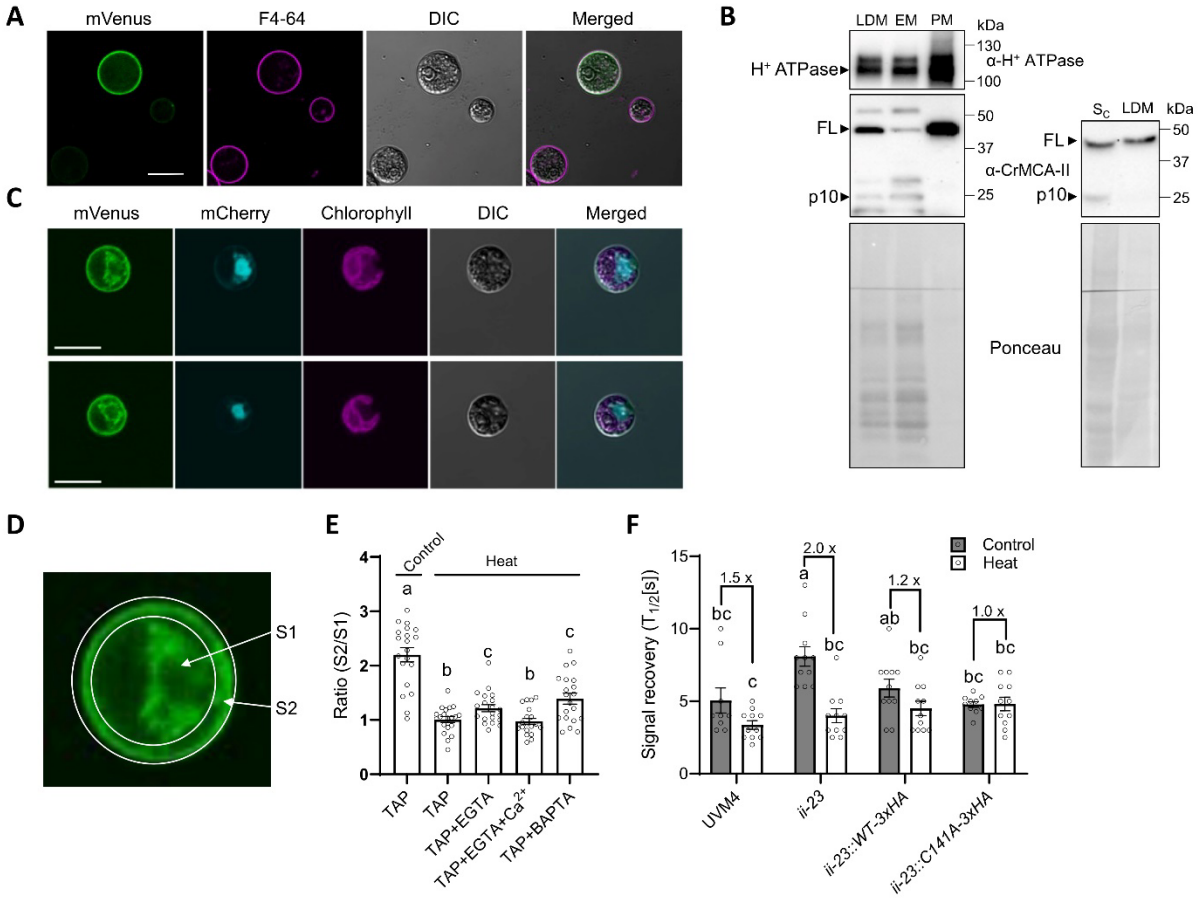

Figure 5 CrMCA-II is localized to the PM and modulates its fluidity. **A.** The PM localization of CrMCA-II-mVenus (green) in unstressed UVM4 cells (grown at 23°C). Cells were stained with FM4-64 (magenta). Scale bars, 10 µm. **B.** Immunoblot analysis of H^+ ATPase and CrMCA-II in different sub-cellular fractions prepared from unstressed UVM4 cells. LDM, low-density membrane fraction; PM, plasma membrane fraction; EM, endomembrane fraction; S_c, concentrated soluble proteins. Ponceau staining was used as a loading control. FL, full-length CrMCA-II. **C.** The PM-to-cytoplasm translocation of CrMCA-II-mVenus (green) after HS at 42°C for 60 min. Cells co-expressed mCherry-NLS (turquoise). Scale bars, 10 µm. **D.** Separation of the whole cell area into the cytoplasm area (S1) and PM area (S2) for CrMCA-II-mVenus PM-to-cytoplasm signal ratio quantification in **E. E.** The PM-to-cytoplasm ratio of CrMCA-II-mVenus in unstressed (23°C, Control) and heat-stressed (42°C, Heat) cells grown in TAP medium (0.34 mM $CaCl_2$) with or without EGTA (0.75 mM), BAPTA (0.5 mM), or simultaneous presence of both EGTA (0.75 mM) and $CaCl_2$ (1 mM). **F.** Recovery rate of fluorescence signal of DiOC6(3) following photo-bleaching (FRAP) of cells from indicated strains grown under no-stress conditions (23°C, Control) or HS (39°C for 60

min, Heat). Numbers on the top of the chart indicate fold-increase of PM fluidity in heat stressed compared to unstressed cells. Data in **E** and **F** represent the means ± SEM from at least three independent biological replicates, each containing at least 3 individual measurements (cells). Different letters indicate significant differences at $p < 0.05$ (a two-way ANOVA with Tukey's honest significant difference test).

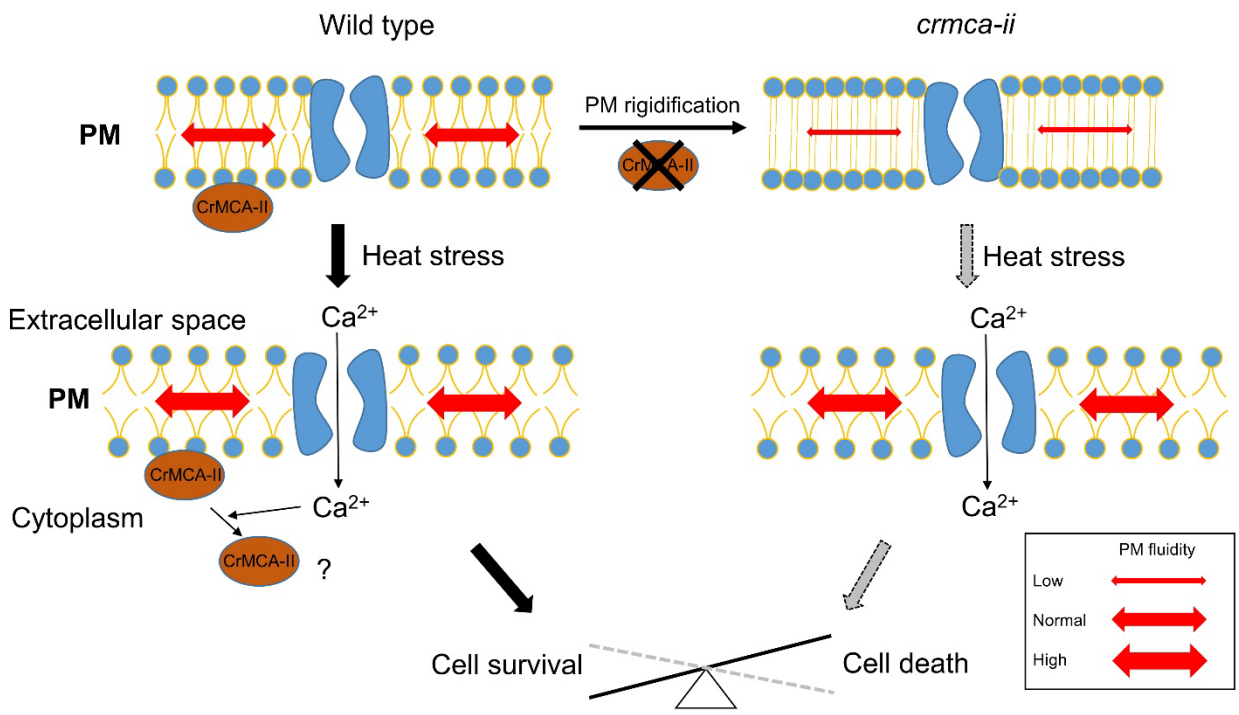

Figure 6 Hypothetical model for the CrMCA-II-dependent regulation of thermotolerance. Under favorable growth conditions, CrMCA-II is preferentially present as a zymogen attached to the PM and preventing its rigidification through an as yet unknown mechanism. HS elevates the PM fluidity, an increase becoming more dramatic and disrupting viability in the *crmca-ii* cells with rigidified PM, accounting for their decreased thermotolerance. An increase in the PM fluidity under HS stimulates influx of Ca^{2+} (Schroda et al., 2015) which, in turn, mediates the PM-to-cytoplasm translocation of CrMCA-II. The role of the cytoplasmic CrMCA-II under HS and, in particular, whether it contributes to cytoprotection remains unknown.